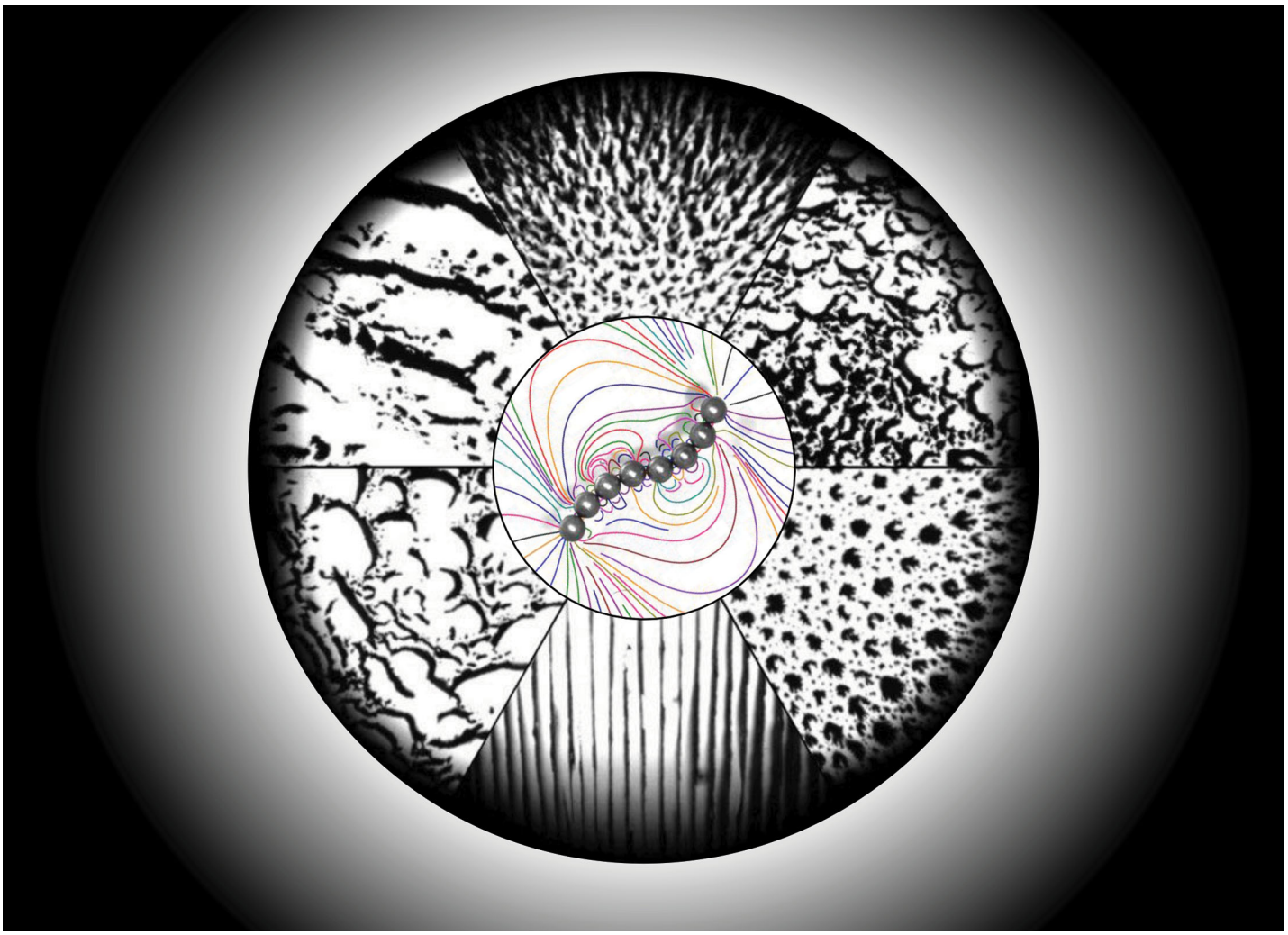

Highlighting research performed in the group of Prof. Juan de Vicente from the Biocolloid and Fluid Physics Laboratory, University of Granada.

Magnetorheology: a review

Understanding the rheological behavior of magnetic colloids under unsteady triaxial magnetic fields. Magnetorheological (MR) composites are smart materials with magnetically controllable mechanical properties. This review paper by Morillas and de Vicente summarizes some of the most relevant publications in the field in the last ten years. The family tree is described and new opportunities presented.

As featured in:

See Jose R. Morillas and Juan de Vicente, *Soft Matter*, 2020, **16**, 9614.

ROYAL SOCIETY OF CHEMISTRY

rsc.li/soft-matter-journal

Registered charity number: 207890

Soft Matter

REVIEW

View Article Online
View Journal | View Issue

Check for updates

Cite this: *Soft Matter*, 2020, **16**, 9614

Received 12th June 2020,
Accepted 31st August 2020

DOI: 10.1039/d0sm01082k

rsc.li/soft-matter-journal

Open Access Article. Published on 01 September 2020. Downloaded on 2/15/2026 12:16:02 AM.
This article is licensed under a Creative Commons Attribution 3.0 Unported Licence.

Magnetorheology: a review

Jose R. Morillas and Juan de Vicente *

Magnetic Soft Matter is a rapidly evolving discipline with fundamental and practical interest. This is due to the fact that its physical properties can be easily controlled through external magnetic fields. In this review paper, we revisit the most recent progress in the field (since 2010) emphasizing the rheological properties of these fascinating materials. New formulations and flow kinematics are discussed. Also, new members are integrated into the long-lived magnetorheology family and suggestions are provided for future development.

1. Introduction

1.1. MR family

Magnetorheology is the science dealing with the rheological properties of magnetorheological (MR) materials. MR materials are magnetic field-responsive multi-phased systems. They generally consist of a magnetizable solid phase dispersed in a non-magnetic carrier that can be either a liquid (so-called MR fluids, MRFs) or an elastomer (so-called MR elastomers, MREs).[1] Currently, special emphasis is given to the case of MR materials prepared in rheologically more complex media (so-called non-Newtonian fluids) such as plastics, shear thinning, shear thickening and/or viscoelastic media. These media bridge the gap between classical purely Newtonian and perfectly elastic carriers used in the formulation of MRFs and MREs, respectively. In this review paper we will refer to them as generalized MR materials (GMRMs). Apart from GMRMs, other emerging MR materials are MR foams, MRF impregnated composites and hybrid MR materials. Fig. 1 summarizes currently existing MR materials.

The origins of magnetorheology are linked to **MRFs** (see Section 2).[2] MRFs exhibit a liquid-to-solid transition under the application of a magnetic field. Their major characteristic is a field dependent yield stress (*i.e.* a minimum stress is needed for the MRF to flow). This property is commonly expressed by the so-called relative MR effect that is defined as the ratio between the stress increment under field and the stress value in the absence of the field. It is important to remark that the MR effect depends both on the on-state (magnetization level M and particle volume fraction ϕ) and on the off-state properties (viscous dissipation within the carrier) of the material.

Since the particles within a MRF sediment in short time scales due to the density mismatch between the particles and the carrier, the interest quickly moved toward **MREs** (see Section 3). In this case, the particles are entrapped within an elastomeric matrix and sedimentation is hindered. Now, the price to pay is a much smaller relative MR effect measured, in this case, as the ratio between the storage modulus increment under field and the storage modulus value in the absence

Biocolloid and Fluid Physics Group and Excellence Research Unit 'Modeling Nature' (MNat), Department of Applied Physics, Faculty of Sciences, University of Granada, C/Fuentenueva s/n, 18071 – Granada, Spain. E-mail: jvicente@ugr.es

Jose R. Morillas received a BSc degree (2014) and a PhD degree (2019) in Physics from University of Granada (Spain). He was recipient of a FPU Predoctoral Fellow to complete his PhD studies on magnetorheology in the pre-yield regime. His research interests include the experimental and numerical characterization of ferrofluids and magnetorheological fluids.

Juan de Vicente received PhD degrees in Physics from the University of Granada (Spain) and the University of Nice-Sophia Antipolis (France) in 2002. He has been FPU Predoctoral Fellow, Marie Curie Postdoc and Marie Curie ERG Fellow at the LPMC-CNRS (France), University of Twente (The Netherlands), University of Wisconsin (USA), Unilever (UK) and Imperial College London (UK). He is recipient of the "Young Investigator Award" from the Social Council and the "Physics Research Award" from the Academy of Sciences. He is presently Professor of Applied Physics at the University of Granada. His research interests include magneto-rheology and soft-elasto-ferrohydrodynamic lubrication.

This journal is © The Royal Society of Chemistry 2020

Open Access Article. Published on 01 September 2020. Downloaded on 2/15/2026 12:16:02 AM.
This article is licensed under a Creative Commons Attribution 3.0 Unported Licence.

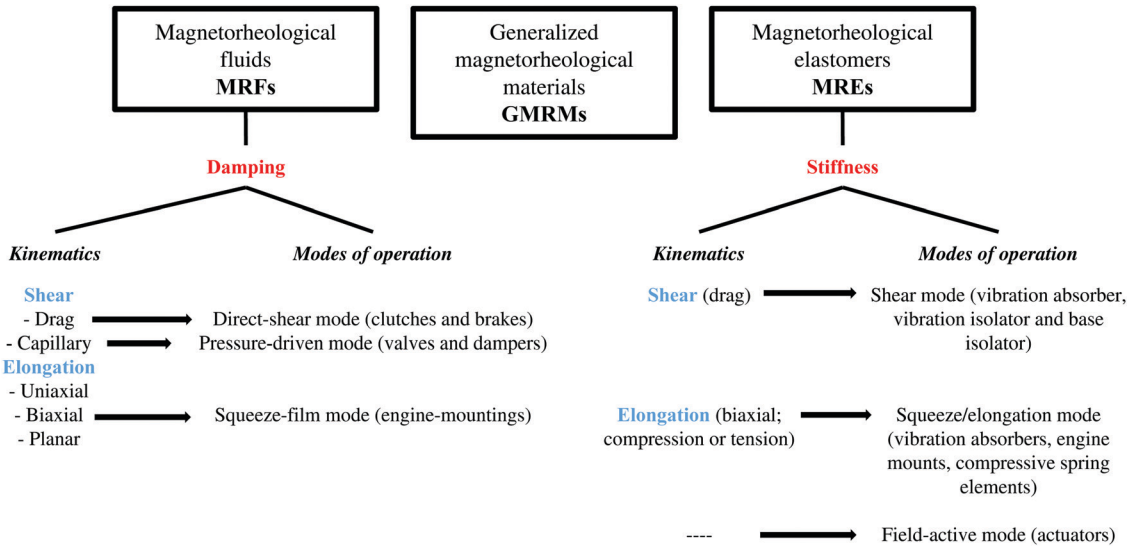

Fig. 1 Overview of MR materials, major characteristics, kinematics and modes of operation.

of the field.[3] The major characteristic of any MRE is the stiffness and loss factor (also called damping factor). Both of them are dictated by M, ϕ and the viscoelastic properties of the matrix.

More recently, novel MR materials have appeared in the intermediate region between fluids and elastomers. These novel formulations fully prevent particle settling without diminishing the MR effect (see Section 4).

Eventhough MR materials are definitely not newcomers, there is still today substantial interest in further developing these materials from practical and fundamental points of view. They already serve as interfaces between electronic and mechanical devices in multiple applications.[4,5] Additionally, they serve as model systems (with easily tunable interparticle interactions) for a better understanding of directed colloidal self-assembly[6] and glass transition.[7]

Currently there exist many review papers in this field of research[8–19] as well as some books.[20–23] The present review paper solely focuses in the most recent advances since 2010. In writing this review we have carefully revised upwards of 3000 publications in JCR journals. We hope that this review will allow to shed light on new directions for fundamental research and foster novel applications in this field.

1.2. Synthesis of magnetic particles

Any MR material is constituted by at least three components: particles, carrier and additives. Usually, the particles are magnetically responsive micron sized carbonyl iron powders (CIPs) and both the carrier and the additives are not magnetic. Besides CIPs, among the many methods described in the literature to synthesize magnetic particles (*e.g.* Singamaneni *et al.*[24]), clearly the majority of publications in the last ten years make use of **hydro- and solvothermal methods**. Interestingly, with these methods it is possible to easily obtain particles with controlled **chemistry** (magnetite,[25] Ni–Zn ferrite,[26] cobalt[27]), **size**[28–30] and **shape** (spherical,[25] octahedral[31] and flower like[27]). Moreover, hydrothermal methods have also been successful in the fabrication of **hollow** magnetic particles.[32]

Other methods and syntheses modifications apart from hydro- and solvothermal ones have also been reported in the formulation of MRFs. For instance, Berasategi *et al.*[33] used the **electric explosion of a wire** to fabricate iron nanoparticles with a saturation magnetization larger than that of CIPs and a high production rate. Noma *et al.*[34] used **arc plasma** to fabricate spherical crystalline Fe nanoparticles of 100 nm diameter and a saturation magnetization of 190 emu g^{-1}. Arief and Mukhopadhyay used **polyol methods** to synthesize $Co_{0.9}Ni_{0.1}$ particles of 450 nm diameter[35] and **hydrothermal reduction** to fabricate CoNi nanoplatelets.[36] Nickel **nanowires** were fabricated by Xia *et al.*[37,38] using a one-step synthesis method. **Composite magnetizable polymeric particles** were synthesized by Rodriguez-Lopez *et al.*[39] using micro-fluidic devices and by Kim *et al.*[40] using mini-emulsion polymerization. These composite particles consisted of micronsized polymeric particles with nanosized magnetic inclusions. Finally, **magnetic carbon nanoparticles** were also synthesized by Lee *et al.*[41] through carbonization of iron-doped polypyrrole nanoparticles.

1.2.1. Post-treatment, surface functionalization and additives. Once the particles are synthesized, it is frequently needed to subject them to a post-treatment[42,43] and/or to carry out their surface modification.[44,45] Moreover, when dispersed in the carrier it is also convenient to incorporate additives. Without weakening the MR effect too much, one can improve the compatibility with the carrier, the sedimentation stability, the tribological properties, prevent interparticle aggregation in the off-state, *etc.* A comprehensive review paper on the preparation of MRFs is that of Ashtiani *et al.*[46] In their paper, special emphasis is paid to the sedimentation stability implications and MR effect. A more recent review paper is that of Seo *et al.*[47] This particular review paper is more focused on the progress of coating approaches of CIPs, especially with foamed polystyrene (PS) layers.

Open Access Article. Published on 01 September 2020. Downloaded on 2/15/2026 12:16:02 AM.
This article is licensed under a Creative Commons Attribution 3.0 Unported Licence.

The influence of **annealing temperature** in the magnetic properties of the particles was investigated by Sedlacik *et al.*[43] A larger annealing temperature resulted in a larger particle magnetization. Also, the influence of **plasma treatment** of CIPs in the suspension stability was reported by Sedlacik *et al.*[42] An enhanced stability resulted from the interactions between the fluorine bonded on the CIPs surface and methyl groups of the silicone carrier oil. The influence of **fatty acids** (lauric, myristic, palmitic and stearic acid) on the stability and MR effect of silicone-based MRFs was investigated by Ashtiani and Hashemabadi.[48] They observed an enhancement when increasing the carbon chain length of the acids. More recently, **superplasticizer** molecules have also been used in the formulation of MRFs in an attempt to reach extremely high particle loadings.[49]

2. Magnetorheological fluids (MRFs)

Magnetorheological fluids (MRFs) were the first in the big MR family to be discovered. Review papers on MRFs are those of Rankin *et al.*,[8] Klingenberg,[9] Bossis *et al.*,[10] Bica,[11] Goncalves *et al.*,[12] Park *et al.*,[13] de Vicente *et al.*,[14] Ghaffari *et al.*[16] and Felicia *et al.*[18]

2.1. Post-yield regime

When magnetized at rest, MRFs self-assemble forming structures oriented in the field direction. However, when a sufficiently strong stress is superimposed (above the so-called yield stress), these structures break and the MRF flows. Hence, MRFs are said to behave as solids in the pre-yield regime and as liquids in the post-yield regime. In practice, MRFs always operate in the post-yield regime.

2.2. Yield stress

The mechanical behavior of MRFs is dictated by the magnetic field-induced structures and they are characterized by a single magnitude: the yield stress. Two yield stresses are generally distinguished in this field: the static and the dynamic yield stress. On the one hand, the **static yield stress** can be defined as the upper stress limit of the pre-yield regime, *i.e.* the maximum stress that the MRF can support when it is strained elastically, without implying sample flow. On the other hand, the **dynamic yield stress** can be seen as the stress level at the onset of the post-yield regime. In this scenario, the sample is flowing but at very small shear rate. Thus, the time scale related to particle rearrangement is totally driven by the magnetic forces but not by the hydrodynamic forces. As a result, at low shear rates the MRF stress level is independent of the shear rate, that is, there is a plateau in stress or a (dynamic) yield stress. The final goal in MRF technology is to achieve the largest MR effect possible and therefore the largest yield stress.

2.3. Challenges: stability

For any MRF to be of interest in practical applications, it must exhibit a low off-state viscosity, be easily redispersable, be stable (in terms of chemical and sedimentation stability) and be resistant against chemical corrosion and/or wear.

Undoubtedly, a major problem in MRFs is that the particles suffer from **sedimentation instability** because of the density mismatch between them and the carrier. By both increasing the viscosity of the carrier or reducing the density difference it is possible to slow down the sedimentation.

Apart from being kinetically stable, particles must also be **chemically stable** so that they do not (thermo)oxidize nor corrode under extreme environments. Two recent experimental papers on the importance of oxidation and corrosion are that of Plachý *et al.*[50] and Han *et al.*,[51] respectively. In both cases, saturation magnetization decreased when particles oxidized and/or corroded and therefore the MR performance decreased as well.

Durability is another requirement for MRFs. Desrosiers *et al.*[52] identified base oil expansion and particle oxidation as two degradation phenomena in clutches, and proposed recirculation and expansion volume as solutions. Also, Wiehe *et al.*[53] reported the temperature induced effects on the durability of MRFs. More recently, it has been shown that two mechanisms affect the durability of the MRF depending on its operating point. In the pre-yield regime magnetostatic forces are responsible for particle wear. In the post-yield regime, the degradation mechanism is not clear but seems to be related to thermal/chemical effects in the carrier fluid.[54]

For a recent review on the shortcomings of MR technology we refer to Wahid *et al.*[55]

2.4. Experimental techniques

The **mechanical properties** of MRFs are typically investigated using rheometry. Torsional flows are more frequently used in their rheological evaluation,[10] cake formation is investigated through penetration tests with a blade[56] and redispersibility is studied using vane tools[57] or freeze-sampling methods.[58]

The **sedimentation stability** was traditionally investigated by **visual inspection** first by the naked eye and then with sophisticated equipment that allowed us to track the sedimentation profile (*i.e.* the mudline location) as a function of time. However, by visual observation it is not possible to identify any internal stratification in the MRF although it is now well known that MRFs stratify in four sedimentation zones (supernatant zone, original concentration zone, variable concentration zone and sediment zone) in agreement with the Kynch's settling velocity model.[59]

A major breakthrough in the understanding of the sedimentation behavior of MRFs was the use of **magnetic inductance monitoring techniques**.[60–62] They are based on the magnetic permeability mismatch between the particles and the carrier and the idea that the reluctance of a MRF depends on its particle loading. Hence, after calibration, it is possible to get information on the particle concentration by simply measuring the reluctance. Xie *et al.*[63] and Choi *et al.*[64] used a vertical axis inductance monitoring system (VAIMS) to investigate the sedimentation behavior of MRFs and the four sedimentation zones were identified. More recently, Wen *et al.*[65] reported a refined

 This journal is © The Royal Society of Chemistry 2020

Open Access Article. Published on 01 September 2020. Downloaded on 2/15/2026 12:16:02 AM. This article is licensed under a Creative Commons Attribution 3.0 Unported Licence.

inductance sensor with a low aspect ratio coil to localize rapid changes in concentration. However, a major disadvantage of this technique is that the results depend on the magnetic field strength and that the latter may also induce interparticle aggregation. A solution for this is the use of **thermal conductivity measurements**.[59]

2.5. Formulations

Progress in the formulation of MRFs during the last ten years can be grouped in two categories: core–shell particles and bidisperse MRFs.

2.5.1. Core–shell particles. Simply covering the magnetic particles with appropriate materials in a core–shell structure is clearly the most direct way to improve dispersion stability[66,67] and reduce the effective density of the magnetic particles[68] thus preventing **sedimentation**,[69] **oxidation**[69,70] and increasing **corrosion resistance** to the working environment.[71,72] Additionally, such a coating can provide the particles with a **dual responsive character** (*e.g.* response to external electric fields with a polyaniline (PANI) coating[73,74]) and/or improve the **tribological properties** of the suspensions.[71,75] Of course, the price to pay is a **lower particle magnetization** (if the coating is not magnetic) and, therefore, a lower MR effect as the coating shell gets thicker.

There is a vast amount of publications in the last ten years reporting the synthesis of core–shell magnetic particles for MR applications. Two recent review papers on polymeric coatings are those of Liu *et al.*[76] and Seo *et al.*[47] In Table 1 we show a summary of some of the most recent papers describing the fabrication of core–shell particles.

2.5.2. Bidisperse MRFs. During the last ten years there has been a very active work on the fabrication of MRFs by mixing particles with different characteristics. These are so-called bidisperse MRFs. Traditionally, the main population consists of CIP while the minority population can be very diverse (*e.g.* big or small, spherical or not spherical, magnetically soft or hard, magnetic or non-magnetic, mechanically hard or soft, *etc.*). By using bidisperse MRFs one can **improve dispersion stability**,[95] **reduce the off-state viscosity**,[96] **increase the MR effect**[95,97–101] and **minimize the sedimentation**.[97,98]

First papers in this field explored mixing particles of different sizes (**bimodal MRFs**) with at least one particle in the micrometer range. In these references two main groups can be distinguished depending on the particle diameter ratio between

Table 1 Formulation routes followed by different references in the literature to obtain core–shell particles. Main morphological features are also summarized. MWCNT: multiwalled carbon nanotube

Publication	Core/shell	Size, diameter (nm)	Shape	Preparation method or suppliers
Liu *et al.*[66]	CIP/silica	~4500	Spheres	CD grade from BASF/Stöber
Gao *et al.*[67]	Magnetite/PS	~100	Spheres	Coprecipitation/Shirasu porous glass (SPG) membrane emulsification technique
Sedlačík *et al.*[68]	CIP/PANI	~3500	Spheres	EA grade from BASF/polymerization
Cvek *et al.*[69]	CIP/poly(glycidyl methacrylate) (PGMA)	~2000	Spheres	SL grade from BASF/surface-initiated atom transfer radical polymerization
Mrlik *et al.*[70]	CIP/cholesteryl chloroformate	~2000	Spheres	ES grade from BASF/two step reaction
Lee *et al.*[71]	CIP/PMMA	~4000	Spheres	ISI/polymerization
Esmaeilzare *et al.*[72]	CIP/cerium oxide CeO_2, lanthanum oxide La_2O_3 and praseodymium oxide Pr_2O_3.	~2000/unknown	Spheres	CN grade from BASF/Merck, Alfa Aesar, Sigma Aldrich
Sim *et al.*[73]	Magnetite/PANI	~800	Spheres	Solvothermal and oxidation polymerization
Min *et al.*[74]	CIP/PANI	~2000	Spheres	CC grade from BASF/one step *in situ* oxidation polymerization process
Chen *et al.*[75]	CIP/graphene oxide	~1000	Spheres	CM grade from BASF/Hummers' method
Dong *et al.*[77]	Sepiolite/magnetite	Unknown	Rods	Sigma Aldrich/coprecipitation
Hajalilou *et al.*[78]	CIP/Ag	~1000	Spheres	Unknown/Green method
Kim *et al.*[79]	CIP/polyamide 6	~4500	Spheres	CD grade from BASF/*in situ* polymerization method through a phase inversion method
Kim *et al.*[80]	CIP/PGMA	~2000	Spheres	CC grade from BASF/dispersion polymerization
Kwon *et al.*[81]	CIP/xanthan gum	~5000	Spheres	ISP/solvent casting method
Kwon *et al.*[82]	Magnetite/PANI	Unknown	Spheres	Micelle-assisted self-assembly method
Nguyen *et al.*[83]	CIP/silica	~4500	Spheres	CD grade from BASF/Stöber
Park *et al.*[84]	Magnetite/PMMA	~10	Spheres	Coprecipitation/double miniemulsion method
Park *et al.*[85]	Magnetite/polypyrrole	~500	Spheres	Hydrothermal/*in situ* polymerization
Piao *et al.*[86]	PANI/magnetite	Unknown	Fibers	Chemical oxidative polymerization/precipitation
Chae *et al.*[87]	PS/magnetite	~500	Spheres	Surfactant-free Pickering emulsion polymerization/Sigma Aldrich
Fang and Choi[88]	CIP/MWCNT	~4500	Spheres	CD grade from BASF/using 4-aminobenzoic acid
Fang *et al.*[89]	CIP/PANI/MWCNT	~4500	Spheres	CD grade from BASF/dispersion polymerization and solvent casting
Fang *et al.*[90]	CIP/PS/MWCNT	~4500	Spheres	CD grade from BASF/dispersion polymerization and emulsification
Liu *et al.*[91]	CIP/silica	~4500	Spheres	CD grade from BASF/sol–gel method based on the silane grafted CIP in two steps
Liu and Choi[92]	PMMA/magnetite	~10 000	Snowman	Seeded polymerization/coprecipitation
Liu and Choi[93]	CIP/silica/MWCNT	~4500	Spheres	CD grade from BASF/sol–gel/layer-by-layer
Pei *et al.*[94]	Silica/magnetite	~200	Spheres	Stöber/solvothermal

Open Access Article. Published on 01 September 2020. Downloaded on 2/15/2026 12:16:02 AM.
This article is licensed under a Creative Commons Attribution 3.0 Unported Licence.

the main and minority populations. In a first group, the large-to-small diameter ratio is around 10 so that both populations are non-colloidal in size. Thanks to the sample polydispersity, their main advantage is a smaller off-state viscosity in comparison to monomodal counterparts for the same solid concentration. At the same time, they show a larger on-state yield stress as small particles seem to help larger ones to get structured in more anisotropic aggregates.[102,103] Previous features enhance the MR effect. However, these MRFs suffer from a high sedimentation rate due to the large size of the particles.

The tendency to sedimentation was partially overcome in a second group of works where the minority population is in the nanosized range (large-to-small diameter ratio around 1000). As a consequence, it suffers from Brownian motion interacting with the main population and hindering the sedimentation of the latter. Although these systems are also polydisperse, the fact that one of the populations is Brownian does not guarantee a reduction in the off-state viscosity. What is more, it has been seen that the yield stress in the on-state (mainly borne by the large particle structures) is not improved for any nanoparticle concentration. The reason seems to be a weakening in the primary structure due to the nanoparticles that reduce the interaction between large particles and the typical length of the structures the latter form.[104,105]

More recently, bimodal MRFs with a large-to-small diameter ratio of 100 have been also studied. The key of this formulation consists in the fact that the minority population has now a mean diameter around 100 nm, just in the transition between the magnetic single- and multi-domain regimes. In this boundary regime, particles exhibit a maximum coercive field and with this, superior magnetic properties in comparison to the main population. As a result, magnetic interactions and yield stress are enhanced in the on-state. At the same time, the coercivity is responsible for the formation of core–shell supraparticles with slower sedimentation rate and better redispersibility in the off-state.[106]

The on-state yield stress and the sedimentation profile for bimodal MRFs are plotted in Fig. 2a and b, respectively. These bimodal MRFs are mixtures of CIPs and small particles of different chemical composition in the aforementioned boundary regime. As observed, in Fig. 2a and b, an enhanced yield stress and sedimentation stability occurs for Fe-based bimodal MRFs because nano-Fe has superior magnetic properties than micro-CIP.

Another particularly interesting set of bidisperse MRFs is the case of **dimorphic MRFs**. In a dimorphic MRF the particles differ in shape. Undoubtedly, the better understood dimorphic MRFs are those constituted by spheres and rods. In these systems, due to their shape, rod particles expose a larger wetted area that makes them aggregate to reduce surface energy and experience more contact points with other particles. Both facts give rise to a stress bearing structure that interlocks the spheres forming a secondary structure. As a result, in the off-state both yield stress and sedimentation stability (see Fig. 2b) increase with the rod concentration. In the on-state, the yield stress can be increased as well, probably due to enhanced friction forces and/or larger magnetization values provided by the particle anisotropy. Nevertheless, a limitation in the rod concentration exists due to their inferior magnetic properties (because of the nanometric size of the rods) and also because the rods interfere in the chain formation of the spherical particles (see Fig. 2a).[97,107,108]

There is a vast amount of publications in the last ten years reporting the preparation of bidisperse MRFs. For a recent paper we refer to Morillas *et al.*[109] In Table 2 we show a summary of some of the most recent papers on bidisperse MRFs.

Of course, one can further complicate things by using **tridisperse MRFs** which consist of a mixture of three particles. The literature on these MRFs is very scarce. A paper in 2011 by Bombard and Teodoro,[126] prepared tridisperse MRFs by mixing two CIPs and water atomized iron powder in an attempt to reach high volume fractions keeping the off-state viscosity as low as possible.

2.6. Physical properties

In the absence of magnetic fields, MRFs behave as conventional suspensions in the frontier between colloids and granular media.

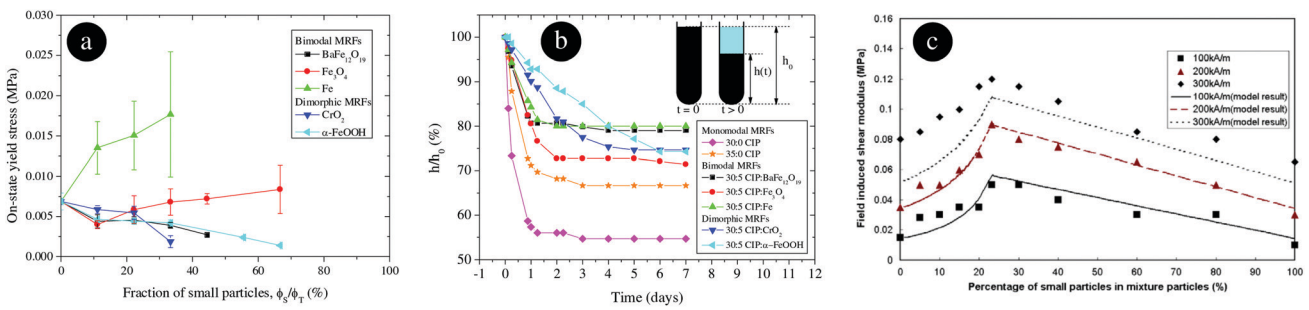

Fig. 2 (a) Yield stress for bimodal and dimorphic MRFs based on micronsized CIP and different small particles. Small particles in bimodal MRFs are in the transition between single- and multi-domain regimes. Small particles in dimorphic MRFs are fiber nanoparticles. The applied field strength is 147 kA m^{-1}. The total particle concentration is fixed at 45 vol%. Adapted from Fig. 4 in ref. 109 with permission from ACS, copyright 2020. (b) Sedimentation profile, in the absence of magnetic fields, for a selected large-to-small particle concentrations of the samples shown in (a). Adapted from Fig. 6 in ref. 109 with permission from ACS, copyright 2020. (c) Magnetic contribution to the storage modulus of a bimodal AMRE as a function of the small particle concentration and the applied field strength. The total particle concentration is fixed at 30 vol%. Points: shear experiments. Lines: effective permeability model prediction. From ref. 305 with permission from IOP Publishing, copyright 2020.

 This journal is © The Royal Society of Chemistry 2020

Open Access Article. Published on 01 September 2020. Downloaded on 2/15/2026 12:16:02 AM. This article is licensed under a Creative Commons Attribution 3.0 Unported Licence.

Table 2 Examples of bidisperse MRFs based on different particle materials. Diameter (spherical), ratio length : diameter (rod) or main size for irregular shaped particles together with the synthesis method or supplier are also indicated

Publication	Materials	Size, diameter (nm)	Shape	Preparation method
Kim *et al.*[95]	CIP/chromium dioxide	~4000/~10	Spheres/rods	CM grade from BASF/unknown
Gudmundsson *et al.*[96]	CIP/CIP	~1000/~1000	Spheres	Various grades from BASF
Jiang *et al.*[97]	CIP/iron	~3500/~50:unknown	Spheres/rods	CN grade from BASF/reduction of Fe^{2+} ion with excessive sodium borohydride in aqueous solution
Powell *et al.*[98]	CIP/CIP/glass	~2000/~8000/~11 000	Spheres	Unknown grade from BASF/BASF/ Potters Sphericel
Armijo *et al.*[99]	CIP/$Fe_{16}N_2$	~1000/~10	Spheres/spheres and cubes	Unknown/green process
Ashtiani and Hashemabadi[100]	CIP/magnetite	~5000/~10	Spheres	Unknown grade from BASF/US Research Nanomaterials
Ashtiani and Hashemabadi[100]	CIP/fumed silica	~5000/~10	Spheres	Unknown grade from BASF/Aerosil
Arief and Mukhopadhyay[101]	Magnetite/iron	~300/~800 : 200	Spheres/nanorod	Thermal decomposition/solvothermal
Morillas *et al.*[106]	CIP/iron	1300/100	Sphere/irregular	EW grade from BASF/US Research Nanomaterials
Sedlačík *et al.*[107]	CIP/iron	~750/~590 : 135	Sphere/rod	HS grade from BASF/surfactant-controlled solvothermal method
Bombard *et al.*[108]	CIP/chromium oxide	3000/nanometric	Sphere/fiber	EW grade from BASF/Sigma Aldrich
Bombard *et al.*[108]	CIP/goethite	3000/nanometric	Sphere/fiber	EW grade from BASF/Bayer
Morillas *et al.*[109]	CIP/magnetite	1300/150	Sphere/irregular	EW grade from BASF/Sigma Aldrich
Morillas *et al.*[109]	CIP/barium ferrite	1300/50	Sphere/sphere	EW grade from BASF/Sigma Aldrich
Arief and Mukhopadhyay[110]	NiCo/~magnetite	~700/~10	Spheres	Polyol/Ferrotec
Esmaeilnezhad *et al.*[111]	CIP/magnetite	~1000/~10	Spheres	CM grade from BASF/precipitation
Jang *et al.*[112]	CIP/maghemite	~7000/~500	Spheres/rods	CM grade from BASF/HR-350 from Magnox
Jönkkäri *et al.*[113]	CIP/maghemite	~1000/~10	Spheres	HQ grade from BASF/LFS method
Klingenberg and Ulicny[114]	CIP/glass	~5000/~10 000	Spheres/hollow spheres	Unknown grade from BASF/Accumet Corp.
Leong *et al.*[115]	CIP/maghemite	~10 000/~10	Spheres	Sigma Aldrich/coprecipitation
Marins *et al.*[116]	CIP/sepiolite	~1000–10 000/ ~20–40	Sphere/rod	Prolabo/Tolsa
Susan-Resiga and Vékás[117]	Fe/magnetite	~2100 ± 1130/~7	Sphere/sphere	Merck/ROSEAL Co. (coprecipitation)
Susan-Resiga and Vékás[118]	Fe/magnetite	~10 000/~6.9	Sphere/sphere	Merck KGaA/coprecipitation
Susan-Resiga and Barvinschi[119]	Fe/magnetite	~10 000/~6.9	Sphere/sphere	Merck KGaA/coprecipitation
Piao *et al.*[120]	CIP/sepiolite	~7000/~10	Sphere/rod	CM grade from BASF/Sigma Aldrich
Chae *et al.*[121]	CIP/attapulgite	~4000/~10	Sphere/rod	CM grade from BASF/Fluorochem
Cvek *et al.*[122]	CIP/carbon allotropes	~2500/~10	Sphere/rod	SL grade from BASF/Sigma Aldrich
Kwon *et al.*[123]	CIP/halloysite	~4500/~100	Sphere/unknown	CD grade from BASF/Sigma Aldrich
Jonsdottir *et al.*[124]	CIP/iron	~2000/~25 and ~2000/~100	Spheres	HS grade from BASF/Nanostructured & Amorphous Materials Inc.
Ngatu *et al.*[125]	Iron/iron	Between 6000 and 10 000/230 diameter, 7500 ± 5100 length	Sphere/nanowire	Alfa Aesar/templated assisted electrodeposition

However, under the presence of a magnetic field, the magnetic constituents in a MR material become magnetized and interact through magnetostatic forces. In the case of MRFs **at rest**, these forces will promote the dynamic self-assembly of the constituents under a deterministic process if they overcome Brownian motion. This criterion is commonly assessed in the specialized literature through the **coupling parameter** λ defined as the ratio between magnetic and thermal energies. The dynamic self-assembly of MRFs in the absence of flow has been investigated using **experiments**,[127,128] **particle level simulations** (CIP,[128] shifted dipoles[129]) and **X-ray micro-computed tomography (XμCT)**.[130] It has been demonstrated that the aggregation process (its time scale) and the aggregate morphology are dictated by the ratio between two length scales. First, the characteristic interparticle distance R_0 in the absence of a magnetic field given by the particle volume fraction $R_0 \sim d\phi^{-1/3}$ (d is the particle diameter). Secondly, the distance R_m where the magnetostatic energy of a pair of particles equals the thermal fluctuations: $R_m \sim d\lambda^{1/3}$. If $R_m < R_0$, the aggregation process is diffusion limited while it will be deterministic in the opposite case. In addition, large R_m/R_0 values imply columnar particle aggregates with defects (not aligned with the field) are more likely than perfectly linear chains.

In the presence of a flow, hydrodynamic forces that try to disperse the particles apart, compete against the magnetostatic ones that promote interparticle aggregation. In fact, a dimensionless number has been documented to describe the rheological response under shearing flow. This is the so-called **Mason number** (Mn) commonly defined as the ratio of the

Open Access Article. Published on 01 September 2020. Downloaded on 2/15/2026 12:16:02 AM. This article is licensed under a Creative Commons Attribution 3.0 Unported Licence.

aforementioned forces in the (hydrodynamic) Stokes' drag and (magnetostatic) dipolar approximations. Under this frame, the equation of motion of the particles is solely controlled by Mn and therefore it appears as a key parameter describing the formation and breakage of the internal structures, and with this, the rheology of the MRF. For small Mn, magnetostatics are dominant. This leads to large and strong particle structures along the field direction. On the contrary, for large Mn magnetostatics is negligible in comparison to hydrodynamic forces. These leads to aggregate breaking and particles flowing.

Overall, three dimensionless numbers (λ, ϕ and Mn) dictate the flow behavior of MRFs.

2.6.1. Shearing flow. In this section we revisit the most recent progress in the understanding of the flow behavior of MRFs under shearing flows. Here, we distinguish between drag and capillary flows.

Under flow and magnetic fields, MRFs essentially behave as plastic materials. For simplicity, the Bingham constitutive equation is preferred but other plastic equations (*e.g.* Casson and Herschel–Bulkley) can better explain the experimental observations because of the nonlinear response when the yield stress is exceeded.[131]

2.6.1.1. Drag flow. Undoubtedly, most of the literature under shearing flow focuses on the understanding of MRFs in drag flows (especially in **plate–plate geometries**) with a **magnetic field oriented in the velocity gradient direction**.[10,132] However, other publications make use of other flow field kinematics and/or magnetic field orientations. The following are some examples. Magnetorheological investigations have recently been performed using **concentric cylinders** to reach high shear rates ($\sim 30\,000\ s^{-1}$) preventing the expulsion of MRF from the gap due to centrifugal forces that are typically observed in plate–plate configuration.[133,134] In this particular geometry, the formation of Taylor vortex flows was reported by Güth and Maas.[134] Furthermore, the magnetorheological behavior of MRFs when the **field is oriented in the vorticity direction** was investigated by Kuzhir *et al.*[135] They reported an unexpected high MR response that was explained by stochastic fluctuations of positions and orientations of the particle aggregates. The fluctuations were modeled as a rotary diffusion process with a diffusion constant proportional to the mean square interaction torque. A quadratic dependence with the particle concentration was found.

Most investigations under shearing flows aim to understand the yielding and flow behavior of MRFs. MRFs **yield** as a result of the fact that the field-induced particle-based structures break under shear. **Confining surfaces** (roughness, gap and magnetic character) are found to strongly affect the yielding behavior of MRFs.[136,137] It has been reported that wall slip cannot always be reliably detected by comparison of the flow curves measured at different gap heights in contrast to classical colloidal suspensions.[137] Also, **multipolar and multibody forces** were demonstrated to play a crucial role at least for perfectly aligned monomodal structures.[138] Being aware of the fact that chain-like structures are **not perfectly aligned** with the magnetic field, Guo *et al.*[139] proposed a yield stress model by introducing an exponential distribution for the orientation angle of the chains. Interchain interactions were neglected in their model.

Once the MRFs yield, their viscosity steadily decreases toward a constant high shear **viscosity** level that is achieved when the particles are randomly distributed in the carrier. The experimental viscosity (normalized by its high shear value) is plotted as a function of Mn for different applied fields in Fig. 3a. Berli and de Vicente[131] demonstrated that viscosity curves are well explained by a **structural viscosity model** that reduces to the Casson model for very large magnetostatic interactions. More recently, Cvek *et al.*[140] investigated the suitability of three constitutive equations to fit the flow curve of magnetized MRFs: Robertson–Stiff, Herschel–Bulkley and Mizrahi–Berk models, by comparing the correlation coefficients, sum of square errors and root mean square errors. The statistical analysis revealed that the best fitting was observed for the **Robertson–Stiff model**. Sherman *et al.*[141] discussed the relationship between the Mn and the Bingham number (Bi) through a so-called critical Mn. This relationship connects the microscopic description of the particle dynamics (Mn) and the macroscopic description of the bulk MRF (Bi). Then, Ruiz-López *et al.*[142,143] showed the functional dependence of the critical Mn on the different control parameters (magnetic field and volume fraction) for MRFs and inverse ferrofluids using experiments and simulations, and eventually provided a master curve. Finally, Jia *et al.*[144] shed some light on how to extend the universal master curve to the case of MRFs formulated in non-Newtonian carriers (see Fig. 3b).

In most cases, the MR effect can be easily enhanced by simply increasing the magnetic field strength† and the particle concentration. The effect of the **magnetic field strength** was reported in the classical papers by Ginder and coworkers[146] and is now better understood for homogeneous and/or saturating fields.[147–149] However, the influence of **particle concentration** is still not well understood yet. A recent overview on the influence of particle loading is that of Bossis *et al.*[150] They benefited from using plasticizer molecules to formulate highly concentrated CIP suspensions ($\phi > 55$ vol%) that were flowable in the off-state. However, they assumed that the yield stress was linear with the particle concentration and this is not in agreement with other publications where the yield stress increases slower than linear for high concentrations.[151] For comparison, in Fig. 3e and f the yield stress scaled by the particle concentration is shown using both experiments and finite element method simulations. In addition, simulations by Morillas and de Vicente[152] showed that a maximum existed (with the volume fraction) in the case of monodisperse particles preassembled in a lattice under affine deformation and saturating fields.

In the last ten years there has been substantial progress on the understanding of the influence of **particle size** on the shearing flow behavior of MRFs. Generally speaking, the bigger the particles the larger their magnetization and hence the

† An exception is the so-called negative MR effect reported by Sakuda*et al.*[145] on elongated particles magnetized along the short axis.

 This journal is © The Royal Society of Chemistry 2020

Open Access Article. Published on 01 September 2020. Downloaded on 2/15/2026 12:16:02 AM.
This article is licensed under a Creative Commons Attribution 3.0 Unported Licence.

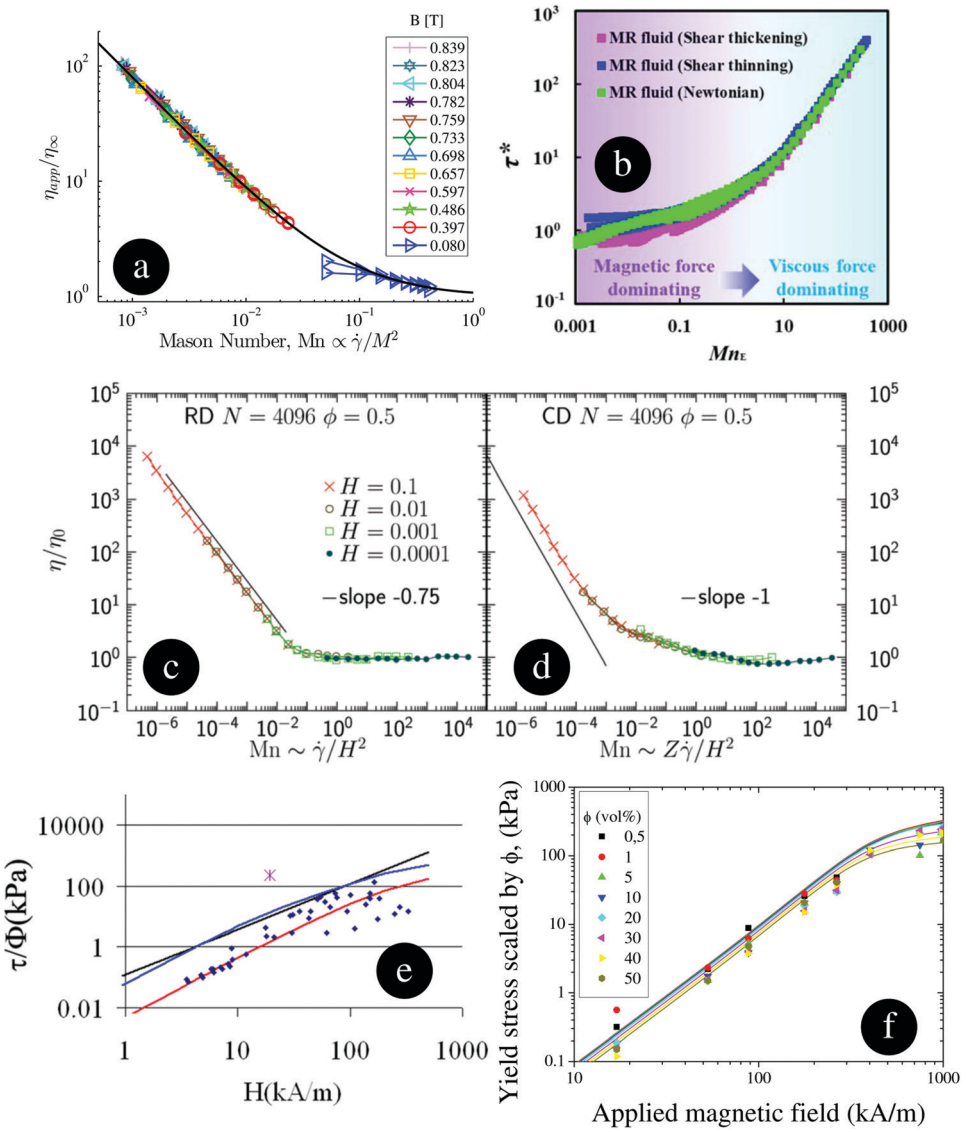

Fig. 3 (a) Experimental viscosity, normalized by its high shear value, as a function of the Mason number Mn, for a commercial MRF (LordMRF-140CG) under different magnetic fields. The black solid line corresponds to the Bingham model equation as fitted to the experimental data. From ref. 141 with permission from Elsevier, copyright 2020. (b) Shear stress normalized by the yield stress as a function of an equivalent Mason number Mn_E, defined as the ratio between viscous and yield stresses. Symbols correspond to MRFs based on CIP dispersed in shear thickening (dispersion of fumed silica in ethylene glycol), shear-thinning (a methyl cellulose solution) and Newtonian (silicone oil) carriers. Adapted from Fig. 3 in ref. 144 with permission from IOP Publishing, copyright 2020. (c and d) Simulated viscosity, normalized by its high shear value, *versus* Mn according to 2D molecular dynamics-like simulations. Two mechanisms for energy dissipation are considered: (c) viscous dissipation due to Stokes drag law and (d) inelastic collisions between particles. Adapted from Fig. 3 in ref. 182 with permission from RSC, copyright 2020. (e) MRF yield stress, normalized by the particle volume fraction, as a function of the applied field strength. Blue points: experiments from the literature on CIP based MRFs with different concentrations. Purple star: shear stress after jamming transition in a high-concentrated (61 vol%) MRF. Red line: finite element method simulations for a pair of particles under affine motion. Black line: analytical model including particle pole saturation and affine motion. Blue line: similar to the red line but supposing that shear happens in a cutting plane. Adapted from Fig. 1 in ref. 150 with permission from Frontiers, copyright 2020. (f) MRF yield stress, normalized by the particle volume fraction, as a function of the applied field for different concentrations. Points: experiments on MRFs based on CIP. Lines: finite element method simulations for a periodic lattice of particles under affine motion. Adapted from Fig. 10 (in ref. 149 with permission from AIP, copyright 2020) and Fig. 9 (in ref. 151 with permission from RSC, copyright 2020).

larger the yield stress.[153,154] Nevertheless, of special interest are those particles that are in the transition between mono- and multi-domain magnetic regimes (particle diameters of around 100 nm). As already stated in Section 2.5.2, these particles exhibit a maximum coercive field and, with this, a superior magnetization and MR effect for the same applied external field than their mono- and multi-domain counterparts.[154]

It has also been reported the influence of **particle shape.** Most of the publications to date concern rod-like particles[155–159] although some publications do discuss plate-like particles as well.[157,160]

Open Access Article. Published on 01 September 2020. Downloaded on 2/15/2026 12:16:02 AM.
This article is licensed under a Creative Commons Attribution 3.0 Unported Licence.

The steady shear behavior of rod-like based MRFs has been described by Bell *et al.*[155] and Gómez-Ramírez *et al.*[158] and the dynamic shear behavior has been reported by de Vicente *et al.*[156] in the linear viscoelastic (LVE) regime and by Kuzhir *et al.*[161] in the non-linear viscoelastic regime. Experiments, simulations and theoretical developments have suggested that rod-like particles exhibit lower sedimentation rate and higher yield stress than spherical ones. Presumably these superior properties were due to a larger interparticle friction and higher magnetization level (lower demagnetization factor for rod-like particles). At present, it is not clear how important both contributions are to the yield stress and a universal explanation is still missing in the literature. Both the shape of the extremity of the rod-like particles[162] and their aspect ratio[159] are crucial to understand the magnetostatic contribution to the yield stress.

Apart from promoting stability, **additives** can also play an essential role in the shearing flow behavior of MRFs. A clear example is that of Bossis *et al.*[49] In their paper, a superplasticizer molecule was used to coat the CIPs and concentrate them in water as much as possible. However, a discontinuous shear thickening (DST) transition appeared as a result of solid interparticle friction under the superposition of small magnetic fields (orders of 10 kA m^{-1}) that pushed the iron particles together and expelled the molecules from the interparticle gap. The critical shear rate associated to the DST phenomena was magnetic field dependent (linearly dependent, see Fig. 3 in their paper). As the magnetic force induced by the field can be easily estimated, it may constitute an elegant approach for a better understanding of the DST phenomenon. Their approach is also useful to generate large changes in viscosity using very small fields.

Traditionally, only shear stresses were investigated in magnetized MRFs subjected to shearing flows. However, with the advent of modern rheometers that are capable to measure normal forces as well, some researchers also moved their attention to **normal stresses** in order to better comprehend the MR mechanism.[163] An easily accessible magnitude in a plate–plate geometry is the normal force acting on the plates due to the MRF. At rest, most of the publications report a quadratic dependence of the normal force with the magnetic field strength in good agreement with the linear magnetization theory. However, contradictory observations have been reported on the shear rate and magnetic field dependence under steady shear flow.[164–166] Chan *et al.*[164] showed that the normal force increased up to a maximum and then leveled off to reach a plateau in a start-up flow test. Liu *et al.*[166] observed a non-monotonous trend in the normal force: with the increase in the magnetic field the normal force increased first, reached a maximum and then decreased to a steady state value. When plotted as a function of the shear rate, the normal force exhibited a minimum. Yao *et al.*[167] investigated the effects of time history, shear rate, and temperature under sweeping magnetic field on the normal force of a MRF. Normal stresses have also been measured under **dynamic oscillatory shear**. Guo *et al.*[168] carried out a systematic investigation using strain amplitude sweep tests and frequency sweep tests. Three regions were identified in the strain sweep mode associated to a LVE region, a nonlinear viscoelastic region and a viscoplastic region. The frequency had little influence on the normal force evolution.

Finally, it should be said that besides rheological properties, other MRF properties have been studied. In particular, both **thermal and electric conductivities** increase when the MRF is magnetized in the field direction. Some recent examples on thermal studies are as follows: Ocalan and McKinley,[148] Yildirim and Genç,[169] Sherman *et al.*[170] and Patel and Upadhyay.[171] Very recently, Ruan *et al.*[172] investigated the influence of oscillatory shear on the magnetic field dependent electric conductivity of MRFs. The conductivity increased about 1500 times when the field increased from 0.06 to 0.96 T. A particle–particle resistance model was also proposed to explain their experimental data.

2.6.1.2. Capillary flow. In this kind of flow, the MRF is forced to pass through a narrow channel. This particular flow kinematics is applicable in the so-called **valve flow mode** in the specialized literature.[173] Early 2011, Kavlicoglu *et al.*[174] proposed an analytical model to predict the pressure loss as a function of the field strength, flow rate and surface topology of the channel in terms of a **non-dimensional friction** factor. The importance of **fluid/wall interactions** in the flow behavior was corroborated by Nishiyama *et al.*;[175] larger pressure drops were measured in grooved surfaces due to the anchoring effect. The importance of **response time** was investigated by Kubik *et al.*[176] In their paper, they described the design, simulation and experimental testing of a MR valve with short response time. Both magnetostatic and hydraulic models were experimentally verified. A novel **radial MR valve** was described by Hu *et al.*[177] In their design the magnetic flux was guided into the annular gap maximizing the effective area and providing larger pressure drops and response times if compared to classical radial MR valves. Also recently, Kubik *et al.*[178] constructed a MRF shaft seal with very low friction torque under a **pinch mode** of operation. A lower friction torque than standard MRFs and a higher burst pressure than any ferrofluid were obtained.

2.6.1.3. Simulations. Many simulations reported in the literature have been successful in predicting experimental data (*e.g.* compare Fig. 3a and d). Lagger *et al.*[179] used 3D **Discrete-Element-Method (DEM)** simulations to investigate the mechanisms of shear stress transmission at the particle level. Particular attention was paid to the wall roughness. In agreement with previous experiments,[136] simulations with ferromagnetic walls showed no influence of wall roughness contrary to the case of non-ferromagnetic walls where the influence of roughness was important. In a subsequent paper by the same authors, an extensive DEM study was performed to elucidate the **rupture mechanisms** behind the yielding process in MRFs.[180] They identified three different patterns: chains, sheets and columns. For each of the three structure types a corresponding failure mechanism was identified. Limitations of their model were (i) the small size of simulated boxes, (ii) that magnetic particles were modeled

 This journal is © The Royal Society of Chemistry 2020

Open Access Article. Published on 01 September 2020. Downloaded on 2/15/2026 12:16:02 AM.
This article is licensed under a Creative Commons Attribution 3.0 Unported Licence.

as magnetic dipoles and (iii) that there was force coupling from the fluid on the particles but not *vice versa*.

This **particle–fluid coupling** was studied together with the influence of the particular hydrodynamic drag force in Lagger *et al.*[181] They investigated three models: a DEM with Stokes drag law for the hydrodynamic interaction and two coupled DEM smoothed particle hydrodynamics models with drag laws from Stokes and Dallavalle/Di Felice, respectively. Currently, this work serves as a useful guideline for the choice of the hydrodynamic interaction model in particle-based MRF simulations. In that respect, Vagberg and Tighe[182] found that the viscous force law affected the **existence of a true yield stress** in MRFs as well. This can be appreciated in Fig. 3c and d; only in the second figure, where energy dissipation is supposed to be related to inelastic collisions between particles, viscosity diverges as Mn^{-1} indicating a yield stress.

Sherman *et al.*[183] described simulations for a **very large number of particles** and demonstrated sheet formation at experimental volume scales. Results showed that the simulation volume had a significant effect on the structures formed. Larger volume sizes promoted the formation of thicker lamellar sheet structures due to the decreased effects of boundary conditions. Sheet formation was inhibited by increasing shear rates and aided by increasing magnetic field strength. Large particle count simulations based on CUDA by the same authors showed that even for narrow particle size distributions, the particle size distribution has a substantial effect in that it dramatically altered chain structures and substantially reduced the stress at low Mn.[184] Simulations on **polydisperse MRFs** were also reported by Ruiz-López *et al.*[185] In this case, the effect of polydispersity was noticeable in the resulting structure but negligible from a rheological point of view.

Aside from magnetic and hydrodynamic interactions, the importance of **non-magnetic interparticle forces** was investigated by Klingenberg *et al.*[186] Non-magnetic forces played a key role in the off-state. However, they played a minor role in the on-state. Wilson and Klingenberg[187] simulated **mixtures of magnetic and non-magnetic particles** in order to explain the yield stress enhancement of these systems as previously seen in experiments.[188] In their analysis they found that non-magnetic particles did not alter the microstructure but formed, together with the magnetic particles, clusters able to transmit stress through contact repulsive forces. Typically, these clusters were aligned in the compression axis and thus they offered a larger resistance to be strained.

Outstanding simulations of **rod-like magnetic particles** are those of Okada and Satoh.[189] They modeled magnetic spherocylinders using Monte Carlo techniques to investigate the structural characteristics of the aggregates and Brownian dynamics simulations to describe their magnetorheological properties.

Finally, capillary flow simulations are scarce in the recent literature. An exception is the paper by Zhang *et al.*[190] In this study, they carried out two-phase Lattice Boltzmann Method (LBM) simulations on the yielding phenomena during **start-up flow of a MRF flowing through a microchannel**.

2.6.2. Elongational flow. In this section we revisit the most recent progress in the understanding of the flow behavior of MRFs under elongational flows. Flows under this title can be divided, at least, into unidirectional monotonous or oscillatory, compression (squeeze) or tension and constant volume or constant area. In particular, most of the publications reported so far correspond to unidirectional monotonous squeeze flow.

The **slow squeeze flow behavior** has been extensively documented in the literature. Early 2011, de Vicente *et al.*[191] carried out experimental tests (under constant volume) and particle level simulations. A micromechanical model was proposed for dilute MRFs[192] while continuum media theory predictions sufficed to explain experimental observations in highly concentrated MRFs.[193] Farjoud *et al.*[194] carried out a mathematical model using perturbation techniques. The compression behavior of MRFs was extensively investigated by Kordonski and Gorodkin.[195] A significant increase in the LVE region was found as a result of column-to-column aggregation assisted by compression of the samples in the field direction. They also investigated superimposed compression and shear deformations. The squeeze flow behavior of MRFs under **constant volume** and uniform magnetic fields was reported by Guo *et al.*[196] They identified two regions: elastic deformation and plastic flow regions. Horak[197] presented a nonlinear model to describe the MRF behavior in the squeeze flow mode. In their work it is assumed **constant area** and no-slip boundary conditions.

Cyclic compression tests were carried out by Ismail *et al.*[198] to interrogate the particle–fluid separation phenomena while Horak *et al.*[199] performed oscillatory compression squeeze mode in a purpose-built experimental setup. A **resonant method** was used by Kaluvan *et al.*[200] to determine the field dependence of the yield stress in MRFs subjected to squeeze flow. According to this method, the viscosity change was measured by the shift in the resonance frequency under a field.

During these last ten years, significant progress has been done in the understanding of the so-called **squeeze-strengthening effect** initially reported by Tao and coworkers.[201] Hegger and Maas[202] proposed a modeling approach that combined the rheological behavior with tribological effects to describe the squeeze-strengthening effect. The squeeze-strengthening of MRFs was carefully investigated by Lucking-Bigué *et al.*[203,204] They derived a Peclet number and adapted it to the Bingham rheological model. This Peclet number well predicted the occurrence of squeeze-strengthening in highly concentrated MRFs. In the second part of their paper, they superimposed squeeze and shear at high speeds. The superimposed rotation affected the squeeze-strengthening by first reducing the radial stress which causes the filtration phenomenon and second by affecting the rate of creation/destruction of the MRF microstructure through the squeeze-to-shear-rate ratio. Horak[197] investigated the squeeze flow of MRFs using simulations and taking into account that the yield stress increases due to compression.

MRFs have also been investigated under **tension**. Because of their tunable yield stress, MRFs can be used for variable-strength controllable adhesion to non-magnetic substrates.[205]

Open Access Article. Published on 01 September 2020. Downloaded on 2/15/2026 12:16:02 AM.
This article is licensed under a Creative Commons Attribution 3.0 Unported Licence.

A model for the MRF **adhesion** under nonhomogeneous magnetic fields was reported by the authors.

Finally, Sadek *et al.*[206] studied the **uniaxial extensional flow** of MRF using a CaBER device with a fixture that is capable to impose a controllable and homogeneous magnetic field over the sample volume, either parallel or perpendicular to the strain direction. Both magnets[207] and coils[206] have been implemented in the setup. It is shown that the filament created during the extensional flow broke earlier when the sample underwent larger Hencky strains (what promoted the capillary forces in the filament) or later when the MRF yield stress was enhanced (either increasing the applied field or particle concentration). Regarding the field direction, fields parallel to the strain made breaking times larger than the perpendicular case due to the more stable configuration of both magnetic field lines along the sample surface and particle structures.

2.6.3. Mixed flows. More complicated flows have also been analyzed. For example, an experimental study on the behavior of MRFs under compression, elongation and shear was reported by Wang *et al.*[208] in a self-constructed test system. Rahimi and Weihs[209] investigated the kinematics of MRFs droplet impact on a smooth surface subjected to a magnetic field using theory and experiments. El Wahed and McEwan[210] investigated the behavior of MRFs in shear, squeeze and mixed (shear + squeeze) modes. They demonstrated that under the mixed mode the behavior was enhanced over those in the squeeze or shear-flow modes. Finally, Pichumani and González-Viñas[211] reported an exotic method to measure the relative viscosity of a MRF by applying a magnetic field during a spin-coating process that involves the evaporation of the solvent.

2.7. Applications

Contrary to other members of the MR family that are still in their infancy, MRFs have successfully **reached the market** in several applications. A recent review on the different applications of MRFs is that of Skalski and Kalita.[212] Other more specialized reviews are focused on dampers,[213] MR valves[214] and robotic applications.[215]

MRFs are traditionally used in **damping applications**. New dampers employing permanent magnets have been constructed by Kim *et al.*[216] and more recently by Lee and Choi.[217] Dampers operating in the squeeze flow regime have also been developed by Gong *et al.*[218] and Sapiński and Gołdasz.[219] Yang *et al.*[220] investigated the behavior of a linear damper containing MR shear thickening fluids exhibiting both MR effect and thickening effect.

Another traditional application of MRFs is their use in **MR brakes**. MR brakes are preferred over conventional hydraulic brakes because the stopping distance and time can be significantly reduced. Patil and Lohar[221] experimentally investigated MR brakes in shear and squeeze flow modes of operation.

The **durability** of a MRF was investigated by Roupec *et al.*[222] It was motivated in the classical papers by Carlson[223,224] that reported an in-use-thickening meaning the damping force increases with the number of load cycles during long-term loading of a MR damper. This was found to be a result of the oxidation of the particles.[225]

MRFs are also of potential interest in **sound propagation applications**. Bramantya *et al.*[226] analyzed the inner structure in MRFs by measuring the ultrasonic propagation velocity. Ultrasonic propagation velocity decreased as the volume fraction of the particles increased. However, when the magnetic field increased, the ultrasonic propagation velocity increased. In a later publication by the same authors, they observed significant differences in the propagation depending on the orientation and mode of application of the magnetic field.[227] Nanda and Karami[228] detailed the possibility of achieving one-way sound propagation using MRFs by subjecting them to a time-space varying magnetic field.

MRFs can be of interest in **thermal transport applications** as well. Forero-Sandoval *et al.*[229] demonstrated that higher concentrations and field strengths led to an increase in the thermal conductivity. Rahim *et al.*[230] explored the influence of adding copper and aluminum to MRFs in their thermal conductivity.

Making use of their adjustable viscosity, MRFs enhance **oil recovery** processes.[231] CIPs have been incorporated to **cement pastes** with the intention to control their rheological properties in the fresh-state in real time[232] and in the fabrication of **MR electrolytes**.[233] More recently, MRFs have been used in the fabrication of **microneedles** using the so-called MR drawing lithography (MRDL) method.[234]

Likewise, MRFs have been used in the fabrication of field **actuated grippers** eliminating the need to supply vacuum.[235] Zhang *et al.*[236] compared the **sealing performance** of MRFs and ferrofluids. A higher sealing pressure was observed for MRFs. For those applications conceived for long operating times, Sato and Umebara[237] proposed a mechanism to control the viscosity of a MRF using solenoids and **permanent magnets** in such a way that no current is needed in the on state while current is solely needed in the off state.

MRFs allow the generation of **liquid drops** with controlled size, shape and **wetting** characteristics.[238] Majidi and Wood[239] showed that **surface micropatterning controlled the interfacial sliding resistance** of MRF at low magnetic fields. Finally, **interfacial patterns** can be tuned by the superposition of magnetic fields in Hele-Shaw cells.[240]

In addition, MRFs are of interest in **tribological applications** with and without abrasive additives. Two examples are surface **finishing and polishing** of freeform (complex 3D) surfaces under the presence of controlled field gradients.[241] A recent review on MR finishing on metals is that of Mutalib *et al.*[242] MR finishing technology is currently commercialized by QED Technologies.[243]

The tribological properties of MRFs **in hard contacts** have been reported in the literature by using reciprocating rigs,[244] wear testers,[245] ball-on-three plates apparatus[246,247] and four-ball tribological devices.[248] Contradictory observations have been reported with no consensus on the influence of magnetic field on the friction and wear scar. Hu *et al.*[248] suggested that the friction coefficient increased and the diameter of the wear

 This journal is © The Royal Society of Chemistry 2020

Open Access Article. Published on 01 September 2020. Downloaded on 2/15/2026 12:16:02 AM.
This article is licensed under a Creative Commons Attribution 3.0 Unported Licence.

scar decreased as the field strength was increased. In contrast, Shahrivar *et al.*[246] observed that both friction coefficient and wear scar slightly decreased upon the application of a magnetic field. The particular magnetic field distribution at the contact seems to play a key role.

In most tribological applications, MRFs are doped **with abrasive particles** like cerium oxide, aluminum oxide and silicon carbide among others.[249] In the presence of magnetic fields, the field-oriented structure holds the abrasive particles at place and restricts the motion of the abrasives. Then, superimposing a relative motion between the MRF and the finishing surface the abrasive particles produce the finishing action. Wang *et al.*[250] modified the geometric shape of the magnets to improve the polishing efficiency. Currently, many **variants of MR finishing** process have been developed to finish different shapes. Some examples are MR abrasive flow finishing (MRAFF),[251] ball end MR finishing (BEMRF),[252] MR jet finishing[253] and lap-MRF process.[249]

3. Magnetorheological elastomers (MREs)

Magnetorheological elastomers (MREs) constitute another key member in the MR family (see Fig. 1). They were created with the aim to avoid sedimentation problems in MRFs. Additionally, they exhibit a superior performance in sealing applications and are more environmentally friendly than MRFs.

MREs are credited to Rigbi and Jilken.[254] In their paper, they reported a pioneering work on a magnetically sensitive elastomer that aimed to exploit the MR effect. However, there seems to exist consensus that the first comprehensive investigation on MREs was conducted by Carlson and coworkers in the 90's.[255]

Similar to MRFs, MREs consist of at least three components: magnetizable (micronsized) particles, a non-magnetic elastomeric carrier and additives. Comprehensive review papers on MREs are those of Li *et al.*,[15] Ubaidillah *et al.*[17] and Cantera *et al.*[19]

The **particles** are typically CIPs. A high purity iron is required for better performance. In fact, a low carbon content in the particles enhances MR effect in dynamic tests.[256] The larger the particle size the smaller (larger) the modulus in the absence (presence) of magnetic fields. The optimal CIP concentration is around 27 vol% in view of theoretical models by Davis.[257]

The **elastomeric (carrier) matrix** is typically made out of silicone rubber, natural rubber or thermoplastic elastomer and prevents the particles from settling. An appropriate matrix should exhibit easy processability, good aging, good thermal properties, and a low elastic modulus to maximize MR effect.

Since CIPs are hydrophilic and matrices are typically hydrophobic, **coupling agents** are frequently used to change the surface of the particles from hydrophilic to hydrophobic. In the off-state and when properly functionalized, CIPs act as conventional fillers reinforcing the matrix and improving its mechanical properties. In MREs, particles are often treated to remove the moisture from their surface before the curing process and to reduce the effect of oxidation on the MREs. Atom transfer radical polymerization (ATRP) techniques are frequently used for surface polymerization of iron particles with fluorinated styrene as monomer in a silicone rubber.[258] A wide range of additives are incorporated in the formulation to enhance the mechanical properties of the MREs. Recently, Aziz *et al.*[259] investigated the influence of several types of processing aids (naphthenic oil, light mineral oil and epoxidized palm oil) in the formulation of MREs.

Depending on how the particles are distributed within the matrix during the crosslinking process, one can distinguish between **isotropic (unstructured)** IMREs or **anisotropic (structured)** AMREs. Particles are homogeneously (randomly) dispersed in the matrix in the case of IMREs. On the contrary, particles are pre-arranged (aligned) in chain-like structures in the case of AMREs. Generally speaking, an anisotropic arrangement gives a better performance than an isotropic arrangement. However, minor differences have been reported between IMRE and AMRE for high-strains (about 100%) base isolation devices when the particle loading was larger than 25 vol%.[260] The advantage of using IMREs instead of AMREs is that they can perform optimally for various directions of vibration. In the literature, the pre-structure process is affected by three main factors: strength of the magnetic field, time exposed and temperature.[17]

3.1. Pre-yield regime

Contrary to MRFs, MREs operate in the pre-yield regime. The mechanical characterization of MREs is generally performed using quasi-static or dynamic tests. Dynamic tests consist of the superposition of small oscillating forces/torques on the samples and measuring the corresponding deformation in the LVE regime. **Two devices are generally used**: torsional rheometers for the shear characterization and Dynamic Mechanical Analyzers or Universal Testing Machines for the compression/tension characterization.

In the preyield regime there are several **operation modes** of interest for MREs: shear mode, squeeze/elongation mode and field-active mode (see Fig. 1). Note that the pressure mode (or valve flow mode) that works for MRFs is not applicable for MREs. However, a new mode exists which is the so-called field-active mode; MREs can change their shape by a magnetic field. For the shear mode and squeeze/elongation mode, MREs work similarly as MRFs. MREs that work in the field-active mode can be used to design various actuators. Examples of shear mode devices include vibration absorbers, vibration isolators, and base isolators. Examples of squeeze/elongation mode devices are vibration absorbers, engine mounts and compressive spring elements.[15]

3.2. Stiffness and damping

Contrary to MRFs that are essentially characterized by a single magnitude, the yield stress dictated by the field-induced structures, MREs are characterized by their **stiffness** and **damping**. Both features come from the viscoelastic nature of the MRE and can be easily interpreted when the MRE is studied in the LVE

Open Access Article. Published on 01 September 2020. Downloaded on 2/15/2026 12:16:02 AM.
This article is licensed under a Creative Commons Attribution 3.0 Unported Licence.

region during oscillatory tests. Under a small sinusoidal strain, the MRE develops a stress (also sinusoidal and with the same frequency) that can be decomposed in phase with the strain or in quadrature with the strain or, equivalently, in phase with the shear rate.

The ratio between the in-phase stress component and the strain is known as the **storage modulus** (in shear or elongation: G' or E') and stands for the instant response of the MRE to a strain. It can be considered a measurement of the **stiffness** or elastic-solid behavior. The ratio between the in-quadrature stress component and the strain is known as the loss modulus (G'' or E''). Since the in-quadrature stress component is, at the same time, in phase with the shear rate, the loss modulus is a measure of the liquid-like behavior of the MRE.[261]

The storage and loss moduli are directly proportional to the energy stored and dissipated by the MRE, hence its **damping** performance (relative to the elastic stored energy) can be measured by the **loss factor** $\tan\delta$, defined as the ratio between the two moduli ($\tan\delta = G''/G'$ or $\tan\delta = E''/E'$).[262]

The **final goal** in MRE technology is to achieve a **large increase of the storage modulus in the on-state** (*i.e.* a large MR effect) and **a controllable loss factor over a wide range of values**. Specifically, in simple vibration control/isolation devices, a small loss factor is required to attenuate oscillations with frequencies above the natural frequency, while a large loss factor is required to attenuate oscillations close to the natural frequency.[263,264]

On the one hand, the majority of the on-state **storage modulus** is dictated by the field-induced structures, particle magnetization and particle concentration. However, the modulus change over its value in the off-state relies also on the viscoelastic properties of the matrix[265] and particle concentration. Experimentally, the most direct way to enhance the MR response is to maximize the particle loading and minimize the storage modulus of the carrier matrix.[266]

On the other hand, Yang *et al.*[267] identified three contributions to the **damping properties (loss factor)** of a MRE: intrinsic, interface and magneto-mechanical damping. Among them, there seems to exist consensus in that the majority of the damping properties come from the second one. At particle–matrix interfaces with a poor adhesion, the frictional sliding between the particles and the matrix is responsible for the energy dissipation. Yet, in some studies, it is stated that the loss factor of the material changes due to the magnetic field. A majority of studies conclude that a magnetic field does not have any remarkable effect on the loss factor.[268–271] Therefore, the most distinctive change in the material property of MREs under a magnetic field is its storage modulus.

Overall, storage modulus and loss factor of MREs are dictated by **three key ingredients**: (i) magnetic field-induced structures (disposition, strength and concentration), (ii) the viscoelasticity of the matrix, and (iii) interfacial adhesion between the particles and the matrix.

In the LVE region, *i.e.* for small deformations typically of the order of 0.01% in torsional shear,[272] both magnitudes G' and $\tan\delta$ remain constant with the deformation amplitude. However, G', G'' and $\tan\delta$ increase with the **frequency** due to the viscoelastic behavior of the elastomer in the rubbery phase (G'',[272] $\tan\delta$[273]). Of especial interest is that AMREs show a larger G' and G'' compared to IMRE and therefore a larger MR effect (assuming the field parallel to the chain axes). It has been experimentally documented that G' increases with the **magnetic field strength** but there is not experimental consensus on the behavior of $\tan\delta$ and there exist opposite experimental results.[274] A weak linear increase of $\tan\delta$ with the magnetic field has been reported by Norouzi *et al.*[273] Lee *et al.*[260] demonstrated that the change in $\tan\delta$ under an external magnetic field was almost negligible compared to the change of G'.

MREs deviate from the linear regime at a **critical deformation** that increases with the excitation frequency[275] but decreases with the **particle loading**,[276] **magnetic field strength** (IMRE[277]) and **temperature**.[276] Once the MRE **deviates from the LVE region**, the moduli decrease with the strain amplitude. This behavior is called the **Payne effect**[278] and is enhanced for the more concentrated MREs.[279]

3.3. Challenges: interfacial adhesion

As shown in the previous section, interfacial adhesion between particles and matrix is crucial for the MRE response. A poor adhesion will allow frictional sliding at the interfaces increasing the loss factor while a good adhesion will prevent the Payne effect, extending the LVE region to larger strains,[17] increasing the storage modulus and reducing the loss factor. Bodelot *et al.*[280] stressed how important the quality of the interfacial adhesion between the filler particles and the matrix was in the mechanical behavior under large deformations.

To improve dispersibility and strengthen interfacial adhesion it is convenient to perform a surface modification of the CIP.[281–283] A few papers exist in the literature demonstrating how to tune the interfacial adhesion, and with it the loss factor, through the use of different additives for the matrix. **Acetone** has been used to prevent iron–silicone attachment and improve the loss factor[284] while **maleic anhydride compatibilizer** in a polybutadiene matrix can reduce interfacial friction and loss factor.[285] In addition, **rosin glycerin** in a natural rubber matrix has shown both behaviors, increasing or reducing the loss factor depending on the used concentration.[286]

3.4. Experimental techniques

Traditionally, **Scanning Electron Micrographs (SEM)** on MRE cutting planes are used to get information about particle structure and interfacial adhesion.[287] More recent approaches involve the use of **microrheology** to monitor MREs curation process in real time[288] and **Atomic Force Microscopy (AFM), Magnetic Force Microscopy (MFM), Force/Distance (F/D) spectroscopy** and **nanoindentation** to obtain information at the surface of the specimen.[289] Undoubtedly, a major breakthrough during the last ten years is the use of **XμCT** to evaluate interfacial adhesion and structuration in MREs.

Odenbach and coworkers were pioneers on the use of XμCT to investigate the 3D internal structure of MREs preserving the

 This journal is © The Royal Society of Chemistry 2020

Open Access Article. Published on 01 September 2020. Downloaded on 2/15/2026 12:16:02 AM.
This article is licensed under a Creative Commons Attribution 3.0 Unported Licence.

integrity of the sample. Some drawbacks of this technique are that, at present, the particle concentration cannot be too high (2 vol%) and the particle size must be big (of the order of tens of microns).[290,291] Fig. 4a shows a typical XμCT image. Using this technique, the influence of the magnetic field on the particle microscopic position and sample macroscopic shape was reported by Gundermann *et al.*[292] Borbáth *et al.*[291] described the structural properties of MREs fabricated at different field strengths. The average number of columns decreased with increasing the magnetic field strength. Particle distributions were obtained by Gundermann *et al.*[293] while Borin *et al.*[294] investigated the influence of particle concentration in the cross-linking of the elastomer. They observed a decrease in the level of crosslinking by increasing the particle concentration. The first investigation on XμCT observations under magnetic fields and a mechanical strain was reported by Schümann and Odenbach.[295]

3.5. Formulations

3.5.1. Ultrasoft MREs. In an attempt to **enhance MR effect**, some interest has been focused in the fabrication of ultrasoft elastomers (storage modulus below 100 kPa).[296] The reason for this is that particles within an ultrasoft elastomer can easily move to form chain-like structures under the presence of a magnetic field. Of course, these MREs are not acceptable in certain applications where a high initial modulus is required because the loading capacity[265] and the durability reduce.[15] Most of the publications can be **grouped in two approaches**: (i) varying the ratio between the monomer and the crosslinker and thus reducing the crosslinking density of the polymer and (ii) softening the polymer by adding a plasticizer molecule.[297] The second approach is preferred because the first one results in a strongly adhesive jelly-like appearance.

Other approaches have also been followed. For example, Forster *et al.*[298] developed a **low-cost wax-based molding technique** to provide certain patterns for ultrasoft (below 40 kPa) MRE surfaces. In Fig. 4b a schematic of the manufacturing process and the resultant patterns are shown.

3.5.2. Multiresponsive MREs. Several attempts are also described in the literature to get multiresponsive MREs that are sensitive to other fields apart from magnetic ones; the most common one being the electric field. These MREs can be integrated into sensors to detect foot motion and in artificial skin.

A strain sensor based on conductive MREs containing silver nanowires in a polyurethane sponge, CIP and PDMS matrix was

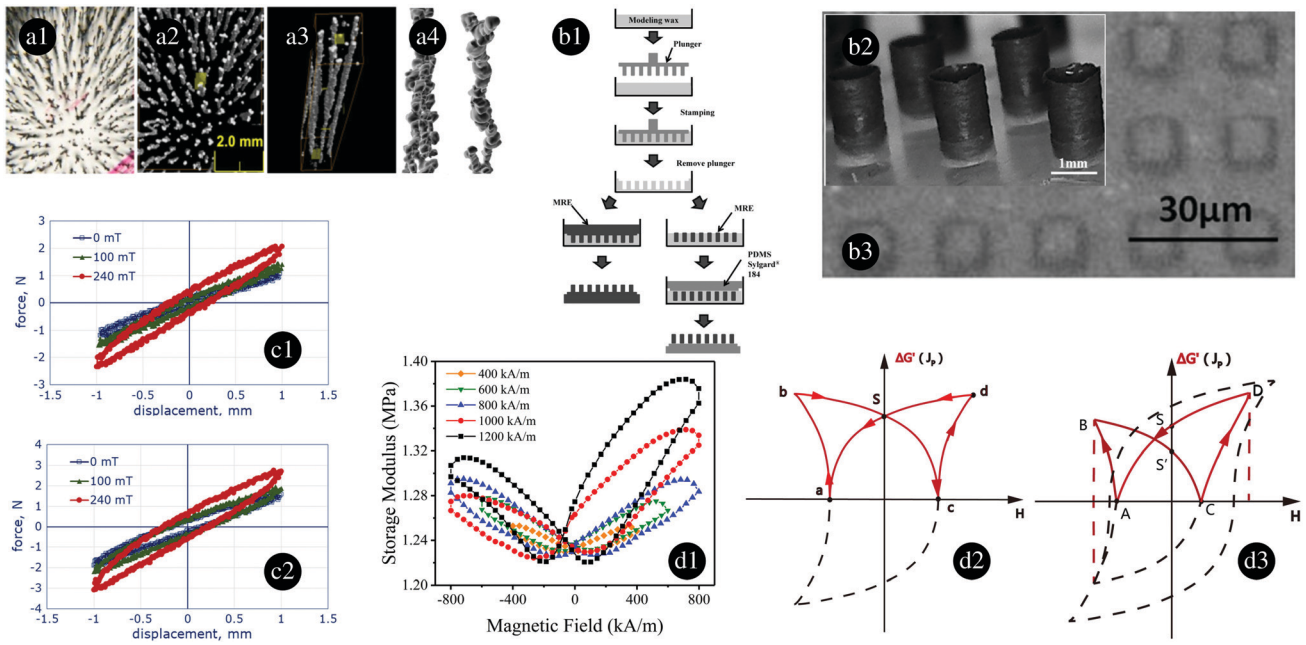

Fig. 4 (a1) Optical microscopy image of an AMRE observed in the direction of the field-induced chains with an applied field strength of 30 kA m^{-1} during curing. (a2) Reconstructed image using XμCT from the same sample as in (a1). (a3) Detail of (a2). The captured box is 15 mm height and 1 × 1 mm^2 cross section. (a4) Detail of chains observed with XμCT. The average particle diameter is around 35 μm. Adapted from Table 1 and Fig. 1 in ref. 291 with permission from IOP Publishing, copyright 2020. (b1) Diagram to stamp MRE patterns over MRE surfaces (left branch) or over surfaces of other materials (right branch). (b2 and b3) Examples of the resultant patterns in perspective and top view, respectively. Adapted from Fig. 2, 4 and 6 in ref. 298 with permission from Wiley Online Library, copyright 2020. (c) Force *versus* displacement loops obtained during tension–compression cycles over a bidisperse IMRE under different applied fields. The total magnetic particle content is 40 vol%. From this, 25% of the particles are hard magnetic: (c1) non-premagnetized sample and (c2) pre-magnetized sample at 1.5 T. Adapted from Fig. 8 and 12 in ref. 311 with permission from Springer Nature, copyright 2020. (d1) Experimental storage modulus during an applied magnetic field loop for an IMRE based on hard magnetic particles (33 vol%). The IMRE is pre-magnetized at different fields indicated in the key of the figure. The loop is asymmetric only if the pre-magnetization field is larger than the maximum applied field in the loop. (d2) and (d3) Schemes showing the loops of magnetization (J_p in this figure-dashed line) and magnetic contribution to the storage modulus ($\Delta G'$-continuous line) when the pre-magnetization field is smaller or larger than the maximum applied field in the loop, respectively. Adapted from Fig. 8 and 10 in ref. 321 with permission from IOP Publishing, copyright 2020.

Open Access Article. Published on 01 September 2020. Downloaded on 2/15/2026 12:16:02 AM.
This article is licensed under a Creative Commons Attribution 3.0 Unported Licence.

developed by Hu *et al.*[299] Prem *et al.*[300] synthesized electro-magneto responsive elastomers by mixing magnetic CIP and electrically conductive particles. Landa *et al.*[301] prepared Ni-based MRE with particles having spherical and rod-like shapes. Then, experiments were recorded compressing the MRE in directions parallel and perpendicular to the needles. Padalka *et al.*[302] investigated MREs filled with Fe, Co and Ni nanowires under oscillatory compressive tests. Both the storage modulus and the dissipated energy per cycle were larger with nanowires than with spheres. Silver-coated magnetite particles were fabricated and dispersed in PDMS by Mietta *et al.*[303] to obtain dual responsive particles. Finally, magneto-electro-rheological elastomers were formulated by Borin and Stepanov.[304]

3.5.3. Bidisperse MREs. Unfortunately, traditional MREs are unsuitable for multiresponsive MREs, and in particular for electric field-responsive MREs, due to their poor conductivity. A solution for this is the use of bidisperse particles. During the last ten years there has been significant progress on the formulation of bidisperse MREs. Table 3 contains some of the most remarkable publications in this field.

Bimodal MREs were probably first investigated by Li and Zhang.[305] Experiments showed that MREs with large particle sizes have lower zero-field modulus and higher field-induced modulus than MREs with small particles. Similar to some bimodal MRFs, bimodal MREs investigated in their work exhibited a much larger MR effect than similar MREs with just one kind of particle (see Fig. 2c). In their paper, they also developed an effective permeability model to describe the behavior of structured MREs.

Li and Sun[265] prepared bidisperse MREs by incorporation of **carbon nanotubes (CNT)** to conventional MREs and demonstrated that both G' and $\tan\delta$ increased with the addition of CNT. The enhancement of G' can be explained bearing in mind that a mechanical reinforcement occurs when adding CNTs. Regarding the $\tan\delta$ increase, it seems that at large CNTs concentrations CIPs aggregate and weaken the bonds with the matrix and increase the loss factor.[314] Indeed, Poojary *et al.*[314] found an optimum CNT concentration below which G' increased and $\tan\delta$ decreased. Similar observations were reported by Aziz *et al.*[312] synthesizing MREs with pristine, carboxylated and hydroxylated multiwalled CNTs as additives below the aforementioned optimum concentration. Finally, Shabdin *et al.*[308] investigated the rheology and resistivity of **graphite** based MREs.

Based on its magnificent performance in the rubber industry (improving elastomers resilience, tear strength and wear resistance strength) **carbon black** has also been widely used in (bidisperse) MRE syntheses. The manuscript by Nayak *et al.*[306] described the fabrication and characterization of MREs containing carbon black in a silicone elastomer. They demonstrated that the addition of carbon black improved the mechanical properties of the MREs. The MR effect was smaller in the case of a hard matrix as compared to a softer matrix. The addition of carbon black attenuated the time rate of mass loss. MREs with carbon black can operate at higher temperature compared to MREs without carbon black. E' and G' increased with the addition of carbon black. Lu *et al.*[309] studied the influence of carbon black on the dynamic mechanical analysis of MREs. In particular, they investigated the storage modulus and the loss factor. They observed that the loss factor increased with the carbon black concentration. Similar results were obtained by Fan *et al.*[310]

Yu *et al.*[264] prepared **dimorphic MREs**. First, CIP was modified by Fe nanoflakes using a simple method and then dimorphic MREs were fabricated by partial replacement of CIP with CIP-nano-Fe. Kwon *et al.*[307] fabricated dimorphic MREs by addition of rod-like maghemite nanoparticles. These MREs exhibited a higher modulus, tensile strength and elongation percentage than pure CIP-based elastomers.

Most of the previous studies on MREs use soft magnetic particles so that the MRE demagnetizes in the absence of an external magnetic field (an exception is the paper by Siegfried *et al.*[318]). However, bidisperse MREs containing **hard magnetic particles** have received significant attention in the last ten years. Lee *et al.*[319] described the preparation of MREs containing γ-Fe_2O_3 rod-shaped hard magnetic particles added to CIP to enhance the MR effect of MREs. Also, Borin *et al.*[311] investigated the mechanical properties of MREs prepared by

Table 3 Examples of bidisperse MREs based on different particle materials. Diameter (spherical), ratio length : diameter (rod) or main size for irregular shaped particles together with the matrix material are also indicated. CNT: carbon nanotube. MWCNT: multiwalled carbon nanotube

Publication	Particles	Matrix	Size, diameter (nm)	Shape
Yu *et al.*[264]	CIP/CIP coated with iron nanoflakes	Polyurethane	~6500/unknown	Spheres
Li and Sun[265]	CIP/CNT	RTV silicone rubber	~15 000/~30 000 : 40	Sphere/fibers
Li and Zhang[305]	CIP	Silicone rubber	~50 000/~5000	Spheres
Nayak *et al.*[306]	CIP/carbon black	RTV silicone elastomer	~5000/unknown	Sphere/unknown
Kwon *et al.*[307]	CIP/maghemite	Natural rubber	~5000/~500:unknown	Sphere/rod
Shabdin *et al.*[308]	CIP/graphite	Silicone rubber	~6000/~16 000	Sphere/unknown
Lu *et al.*[309]	CIP/carbon black	Natural rubber	~3200/unknown	Sphere/unknown
Fan *et al.*[310]	CIP/carbon black	Natural rubber	~3000/~100	Sphere/unknown
Borin *et al.*[311]	CIP/NdFeB	PDMS	~5000/~35000	Spheres
Aziz *et al.*[312]	CIP/MWCNT	Natural rubber	~6000/~10 000 : 10	Sphere/fibers
Aziz *et al.*[313]	CIP/MWCNT	Natural rubber	~6000/~10 000 : 20	Sphere/fibers
Poojary *et al.*[314]	CIP/CNT	RTV silicone rubber	~5000/~10 000 : 20	Sphere/fibers
Sorokin *et al.*[315]	Fe/magnetite	Silicon rubber	55 000/35	Spheres
Aloui and Klüppel[316]	CIP/iron oxide	Styrene–butadiene rubber	3500/15	Spheres/irregular
von Lockette *et al.*[317]	Iron/iron	RTV silicone rubber	40 000/10 000	Unknown

 This journal is © The Royal Society of Chemistry 2020

Open Access Article. Published on 01 September 2020. Downloaded on 2/15/2026 12:16:02 AM.
This article is licensed under a Creative Commons Attribution 3.0 Unported Licence.

mixing soft and hard magnetic particles. Although the MR response is mainly governed by the (easily magnetizable) soft particles, values of E' and $\tan\delta$ in the on-state were larger when hard particles were pre-magnetized (see Fig. 4c). Makarova *et al.*[320] investigated three different hard magnetic particles in the preparation of MREs. Wen *et al.*[321] demonstrated that the storage modulus in a hard MRE can not only be increased by increasing the field but also decreased by increasing the field in the opposite direction. In Fig. 4d1 the storage modulus during applied magnetic field loops is shown. The asymmetric shape comes from the asymmetric hysteresis loops of magnetic particles when the hard MRE is pre-magnetized at a given field and then tested until a smaller applied field (compare Fig. 4d2 and d3).

3.6. Physical properties

In the absence of magnetic fields, MREs behave as conventional filled elastomers. However, in the presence of magnetic fields embedded particles become magnetized and interact increasing the MR effect. This increase is even more noticeable in the case of AMREs if compared to IMREs when the magnetic field is oriented parallel to the direction of the particle chains.[322] Gorman *et al.*[322] is probably the first publication to **compare results for uniaxial and biaxial testing** under high strain fatigue test conditions.

The physical properties of MREs can be described using quasi-static and dynamic tests.

3.6.1. Quasi-static regime. There are three fundamental kinematics to explore the quasi-static regime: shear, tension and compression.

3.6.1.1. Shear. Liao *et al.*[323] described the **influence of shear deformation on the normal force in MREs**. In the quasi-static regime, the normal force decreased with the shear strain at low magnetic field. However, it increased with the strain at high magnetic field. A similar trend was observed in oscillatory shear. However, the normal force decreased sharply when the strain amplitude exceeded 7%. Experimental results for small and large fields were explained in terms of two factors: the elastic modulus in the pre-compression direction and the magnetic torque. The sharp decrease at 7% under oscillatory shear is justified by the breakage of the field-induced structures. More recently, Kikuchi *et al.*[324] investigated the **large strain behavior of MREs** in shear under uniform magnetic fields and compression under non-uniform magnetic fields. Their model was based on the previous model by Kraus.[325]

3.6.1.2. Tension and compression. The tensile properties of MREs have been vaguely investigated in the recent literature. Sandesh *et al.*[326] showed that the tensile modulus of an elastomer increases by addition of CIP. However, it reduced the percentage elongation and tensile strength making the MRE brittle. The tensile properties of magnetically hard MREs were also investigated by Borin *et al.*[327]

Undoubtedly, compression tests clearly dominate over shear and tension tests. The **comparison between tensile and shear moduli** of MREs is missing in the literature. An attempt was carried out by Borin *et al.*[328] using rod specimens. Ghafoorianfar *et al.*[329] proposed a model to predict the **electrical resistivity and magnetostriction of MREs** under different applied magnetic fields and mechanical compressive loads. Han *et al.*[330] proved that the dipole-interaction model failed to explain the tension/compression observed in experiments. In this paper, various filler-chain structures were studied to demonstrate the ultimate field-stiffening effect in MREs. It seems that the wavy chain structure was the key in the modulus increase. The study also foresaw the possibility of a **negative MR effect**. Sun *et al.*[331] described MREs working in **squeeze mode** and proposed a model. Then, in a following publication they compared the shear and squeeze behavior.[332] Interestingly, the squeeze MRE absorber had a larger frequency-shift range than that working in the shear mode. Suo *et al.*[333] proposed a **model for MREs**. An extended fractional-order derivative model was developed to consider the Payne effect using the framework of the Kraus model.

3.6.2. Dynamic regime. Koo *et al.*[334] investigated the dynamic mechanical properties of MREs under **compression**. From the resultant stress–strain loops, they observed that the area of the loop increases as the magnetic field increases, indicating that the dissipated energy in each cycle, *i.e.* the damping properties of the material, also increases. They modeled the dynamic behavior of the MREs by using an **artificial neural network**. Małecki *et al.*[335] studied the dynamic mechanical analysis of MREs of surface functionalized CIP and the **large strain** dynamic mechanical behavior of MREs was investigated by Lee *et al.*[260]

Norouzi *et al.*[273] described the dynamic behavior of MREs in oscillatory **shear** tests in terms of a modified Kelvin–Voigt model. In a later paper, Norouzi *et al.*[336] proposed a MRE model that captures the dynamic behavior in **tensile–compressive** loadings and compared it with experiments. Both the equivalent storage modulus (obtained from the slope of the hysteresis loops) and loss modulus (obtained from the loop area) increased with the field. Guo *et al.*[337] created a model using an **Abel dashpot** for the torsional dynamic oscillatory properties of MREs.

An alternative way to elucidate the viscoelastic character of any material is through the use of creep-recovery tests. In this sense, Qi *et al.*[338] investigated the **creep and recovery** behavior of MREs based on polyurethane/epoxy resin graft interpenetrating polymer networks. Findley's, Burgers and Weibull models were used. In a following paper they investigated the stress relaxation of MREs.[339]

The influence of a **prestress** on the mechanical properties of MREs has also been investigated. Danas *et al.*[340] found that a compressive/tensile prestress made the MRE elongate/compress itself under the presence of a magnetic field (magnetostrictive behavior). On its part, Feng *et al.*[341] have shown that with increasing prestress, both the storage modulus and magneto-induced modulus showed a declining trend after an initial ascent. A theoretical model was also provided in each of these works.

The **temperature** dependence of the dynamic properties of MREs has been reported by Wan *et al.*[342] In their paper, the fractional Maxwell model and the generalized Maxwell model were used.

Open Access Article. Published on 01 September 2020. Downloaded on 2/15/2026 12:16:02 AM.
This article is licensed under a Creative Commons Attribution 3.0 Unported Licence.

3.6.3. Mixed/other regimes. Similar to MRFs, a common trend today is to **superimpose different modes**. In this sense, Tao *et al.*[343] investigated the squeeze-shear mode of operation of MREs. Leng *et al.*[344] described the design, construction and testing of a MRE-based isolator working in shear-squeeze mixed mode. Vatandoost *et al.*[345] described a comprehensive model for the dynamic behavior of MREs under coupled tension–compression mode. The model was capable to describe the asymmetric hysteretic behavior under cyclic deformations.

Also, exotic deformations are attracting the attention of several researchers. For instance, Schubert and Harrison[346] carried out **equi-biaxial tension tests** on MREs. In a subsequent paper, the isotropic and anisotropic magnetic permeabilities of MREs were identified using a simple inverse modelling approach.[347] MREs **under impact loading** conditions were investigated by Leng *et al.*[348] They explored two influential factors: particle arrangement and magnetic field strength. The dissipated energy increased with magnetic field and is larger in the case of structured MREs.

3.6.4. Analytical models. Modelling the rheological behavior of MREs (if interested in their mechanical applications) is the first step toward successful engineering applications. There is currently limited work on the modeling of MREs and can be classified in two different viewpoints: macro-mechanical models based on the MRE force–displacement relationship and micromechanical models describing the MRE at the particle scale.[273] Although micromechanical ones are based in less suppositions, they also entail a higher and commonly unavoidable computational effort when implemented at device (application) scales. In this sense, macro-mechanical models are advantageous as can be easily adapted to the particular application. Nevertheless, they are phenomenological models that do not offer a unique constitutive equation for the MRE rheological behavior (see, for example, Fig. 5a and b).

Among macro-mechanical models, a three-parameter model has been normally used to describe the viscoelastic behavior of rubber-like material. This is typically a combination of a stiffness element and a Kelvin model (*i.e.* a stiffness element and damping element in parallel).[15,273] Most available models in the MRE literature neglect interfacial interactions and therefore their predictions are only appropriate for the storage modulus and not the loss factor. However, as stated in Section 3.2, an appropriate viscoelastic model for MREs needs to capture not only magnetostatic forces but also the viscoelastic character of the elastomeric matrix and the interactions between the particles and the matrix. A model that includes these three contributions is that of Chen and Jerrams.[349] Some of the predictions of this model are shown in Fig. 5c. In particular, it can be seen that the predicted trends for the storage modulus and the loss factor as a function of the interfacial adhesion follow the experimental trends (see Section 3.3).

At particle scale, Li and Sun[274] proposed a micromechanical model that was capable of predicting the off-state stiffness and damping behavior as well as the MR effect in MREs. The dependence of the moduli on the frequency in IMREs was modeled by Agirre-Olabide and Elejabarrieta[275] considering the anisotropy in the magnetic permeability of the MREs. Other theoretical developments are those of Biller *et al.*[350,351] and Vaganov *et al.*[352]

As it happens in MRFs, particle-level simulations have become a very useful tool for MRE modeling (see Menzel[353] for a recent review). With these simulations, it is possible to track each particle position bearing in mind magnetic and matrix mediated forces. An example, among many others, is the work of Pessot *et al.*[354] where they used a simulation to calculate the **frequency-dependent elastic moduli** based on the decomposition of the linear response to an external stress in normal modes. Although they also compared against experiments in Pessot *et al.*,[355] comparisons to validate previous models would be clearly favored by the manual arrangement of iron powder in lattices (*e.g.* Li *et al.*[356] described the analysis, fabrication and characterization of patterned MREs, see Fig. 5d).

3.7. Applications

Commercialization of MR based devices is still limited to MRF dampers and MREs have not penetrated into commercial products.[17] However, classical potential applications of MREs range from automotive[357] and aerospace to civil engineering devices.[291] MREs are traditionally used in mounts and shock absorbers.

Since the pioneering paper by Ginder *et al.*,[268] it was clearly demonstrated the mechanical potential of MREs to develop tuned vibration absorbers. Indeed, today, major potential applications of MREs concern **vibration control (absorption and isolation)**. This is due to the fact that storage modulus and loss factors can be tuned by the superposition of a magnetic field. In particular, the natural frequency of the system increases together with the storage modulus. Of course, in addition to its magnetoelastic character, MREs possess other functions such as magnetoresistance, magnetostriction, piezoresistance and thermoresistance. In particular, the use or MREs in sensing devices is still in its infancy.[299]

The macroscale deformation of magnetized MREs has been studied extensively in the past. However, MREs have recently found another interesting application as the **surface of these elastomers can be micro-deformed** in a controlled way superimposing external magnetic fields. This has an impact in boundary friction, wettability and adhesion properties. Specifically, AMREs that are inherently hydrophobic can become superhydrophobic when a small magnetic field is applied.[358–360] The storage modulus and the surface properties are changed. Chen *et al.*[360] obtained an analytical model for the field-induced surface micro-deformations considering an infinite medium.

Other applications based on surface deformation involve their use as **smart adaptative mirrors**[361] and as **actuator-based hand-held devices** for user interaction with touch screens. Since the touch screen is flat and featureless, the user can only interact with the virtual object under visual guidance and this is a limitation for a blind person. To enhance realism haptic devices based on MR technology are emerging.[362]

MREs are also used in **electromagnetic (EM) protection** applications. Sedlačík *et al.*[363] investigated the EM shielding properties of MREs for the first time. MREs absorbed EM

 This journal is © The Royal Society of Chemistry 2020

Open Access Article. Published on 01 September 2020. Downloaded on 2/15/2026 12:16:02 AM.
This article is licensed under a Creative Commons Attribution 3.0 Unported Licence.

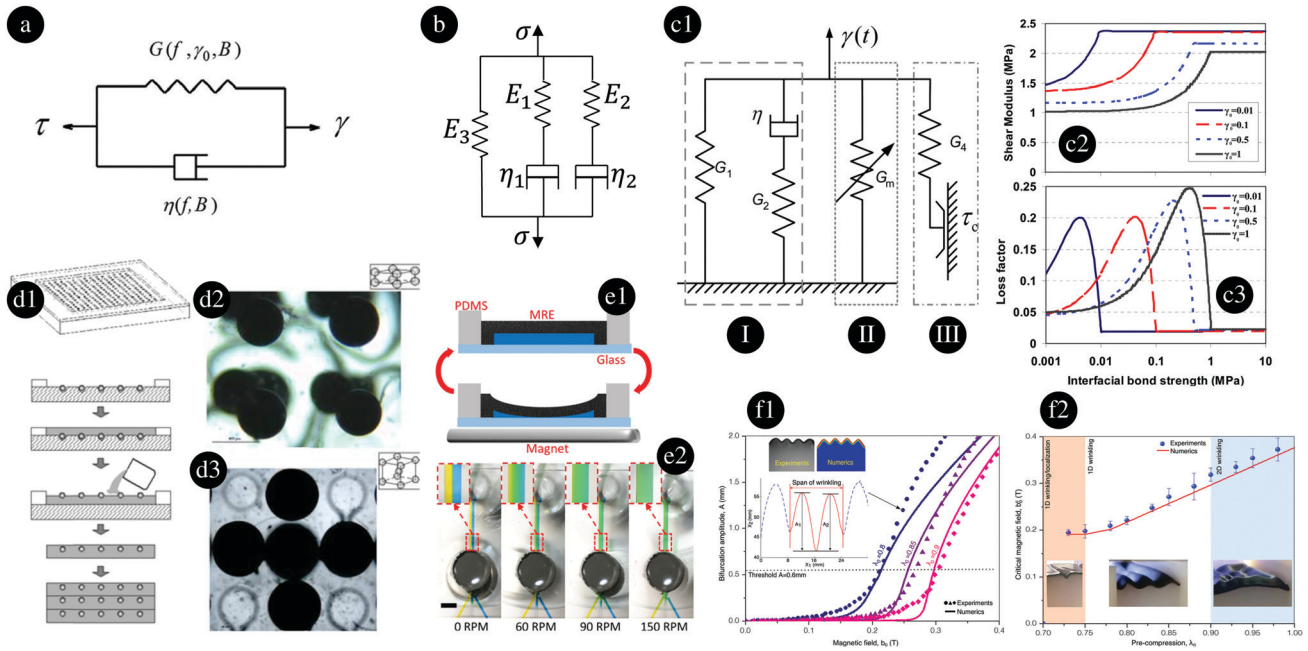

Fig. 5 (a) Model based on stiffness and damping elements as proposed by Norouzi *et al.*[273] to reproduce IMRE behavior in oscillatory shear tests. From ref. 273 with permission from SAGE, copyright 2020. (b) Example of model based on stiffness and damping elements proposed by Norouzi *et al.*[336] to reproduce IMRE behavior in oscillatory compression tests. (c1) Model proposed by Chen and Jerrams[349] for MREs including: (I) viscoelastic properties of the matrix, (II) magnetic contribution to mechanical properties and (III) interfacial adhesion. (c2 and c3) Represent predictions of the storage modulus and loss factor as a function of the interfacial adhesion strength, τ_c in (c1). Adapted from Fig. 1–3 in ref. 349 with permission from AIP, copyright 2020. (d1) Experimental layer by layer protocol to manufacture an AMRE with precise control over particle position. (d2) and (d3) are pictures of the resultant lattice (particles are 400 μm diameter) and body center cubic structures (800 μm), respectively. From ref. 356 with permission from AIP. (e1) MRE actuator implemented in a microfluidic circuit. When a permanent magnet is approached to the MRE, it deforms and squeezes the fluid within the chamber. (e2) Two channels feed the MRE chamber with different colored fluids. By increasing the frequency of approaching the magnet, the MRE induce chaotic fluid motion resulting in both fluids being mixed. Adapted from Fig. 4 in ref. 374 with permission from WILEY-VCH, copyright 2020. (f1) Amplitude of the surface deflection as a function of the applied magnetic field for different mechanical compressions. Magnetic field is applied vertically while the compression is exerted in the horizontal direction in the inset picture. (f2) For a given mechanical compression, the corresponding surface roughness appears above a critical magnetic field. From ref. 382 with permission from RSC, copyright 2020.

radiation in the ultra-high frequency band, namely the range from 700 MHz to 1.6 GHz. The performance was strongly dependent on the magnetic field strength with AMREs exhibiting superior EM shielding than their IMREs counterparts.[364,365] Moucka *et al.*[366] reported the **dielectric properties** of MREs. This is essential for applications such as **piezoresistive sensors or radio-absorbing materials**. It is based on the fact that AMREs exhibit higher electric conductivity when compared to their isotropic analogues. The aim of their work was to correlate the microstructure of the MRE and its dielectric response.

MREs can be applied as anisotropic **thermal, electric and sound conductors/attenuators** as well. Zhong *et al.*[367] investigated the enhancement of thermal transport in AMREs with the flash method. Zhu *et al.*[368] investigated the conductivity of MREs under pressure while their acoustical properties have been recently tested by Hasheminejad and Shabanimotlagh[369] and by Korobko and coworkers.[370]

Apart from a controllable storage modulus and loss factor, MREs also exhibit a **change in shape** when placed under a magnetic field. The field-active mode originates from the magnetostrictive behavior of MREs. Therefore, they can be used in soft actuators and artificial muscles. For a recent review on this topic we refer to Elhajjar *et al.*[371] MREs are currently used as building blocks in sensors and actuators for applications in microfluidics such as self-powered magnetic field sensors,[372] mechanical actuators[373,374] (see Fig. 5e), and micropumps.[375] The influence of temperature in the magnetostriction was investigated by Diguet *et al.*[376] Using digital holographic interferometry, Gong *et al.*[377] showed that there is not consensus on whether an MRE should contract or stretch when a magnetic field is superimposed. The results demonstrated that some regions stretch while other regions contract. Isolated particles in the MRE led to contraction while grouped particles led to stretch.[378] This characteristic makes it possible to control surface roughness and therefore wettability and friction as commented above.

A fast growing field of research is the use of MREs in **tribological applications**. Li *et al.*[379] demonstrated that IMREs exhibit a decreasing friction coefficient with the applied magnetic field. On the other hand, the influence of magnetic field on AMREs is not monotonic. Lian *et al.*[380] studied friction and wear properties of MREs under vibration conditions. Friction was found to decrease with magnetic field and amplitude and to increase with vibration superposition and frequency. Wear depth decreased under fields and increased with vibration.

Open Access Article. Published on 01 September 2020. Downloaded on 2/15/2026 12:16:02 AM.
This article is licensed under a Creative Commons Attribution 3.0 Unported Licence.

Lian *et al.*[381] investigated the stick-slip characteristics of MRE against aluminum plate. Stick-slip is originated from the difference between the static and dynamic friction forces. Controlling stick-slip is important because it can lead to vibration, noise and wear reducing the lifetime of friction pairs. Although it was not relevant at low speeds it enhanced as the speed increased. The superposition of a magnetic field was capable to reduce the stick-slip phenomena and therefore reduce wear as well. The active control of surface roughness in MREs was also investigated by Psarra *et al.*[382] Their experimental system consisted in an IMRE layer deposited on top of a non-magnetic elastomer that served as a substrate. By changing the applied mechanical compression and magnetic field over this system they obtained, experimentally and numerically, a phase diagram organizing the different observed surface roughness patterns (see Fig. 5f).

4. Bridging the gap between MRFs and MREs

Whenever the carrier is neither a Newtonian liquid nor a perfectly elastic material, the MR composite is said to be in the borderline between MRFs and MREs. MR materials in this region constitute a big family that grows quickly with time. We will call them **generalized magnetorheological materials (GMRMs)**. These kinds of materials are referred in the literature as MR gels, MR plastomers, *etc.* (see Fig. 6a taken from Wang *et al.*[383]).

The motivation behind efforts filling the gap between MRFs and MREs is that both kinds of materials are complementary. MRF devices mainly possess variable **damping** while MRE devices mainly have variable **stiffness**. A difficulty that arises when working with GMRMs is that the rheological behavior is in many cases not reversible and this complicates the analysis (*e.g.* MR plastomers). Additionally, the rheological behavior is not linear anymore. Two recent examples exploring the **large-amplitude oscillatory shear (LAOS)** behavior of GMRMs are those of An *et al.*[384] and Pang *et al.*[385] An *et al.*[384] prepared MR materials in **self-assembled triblock copolymers**. They found that the onset strain towards nonlinear rheology decreases substantially under magnetic fields. In their turn, Pang *et al.*[385] measured the normal stress in MR materials prepared in **polyurethane gels** using experiments and particle level simulations. As the amplitude of the strain increased, the peak of the normal stress increased and the trough decreased. Two arguments were provided to explain the normal force evolution: the Poynting effect and the magnetic-induced normal stress.

The use of a non-Newtonian matrix, and in particular a **yield stress material**, has been demonstrated to be very effective in the prevention of particles from sedimentation.[386,387] The paper by Rich *et al.*[388] makes use of the fact that the process of assembling particles into organized functional structures is influenced by the rheological properties of the carrier and in particular its yield stress. Tuning these properties, for example through changes in the temperature as it was done in Wang *et al.*,[389] represented a viable approach for controlling particle assembly. Yang *et al.*[390] prepared MRFs by dispersion of CIP in 12-hydroxy stearic acid (12-HAS) oil solutions as carrier. These suspensions exhibited a remarkable sedimentation stability.

Available literature on this topic can be classified in two main groups: bidisperse and plastomer GMRMs. These systems are usually tested in shear and elongation modes, although some works can be found in valve flow mode as well, *e.g.* Whiteley *et al.*[391]

4.1. Bidisperse

Similar to MRFs and MREs, the use of bidisperse GMRMs exhibits benefits over monomodal systems, in particular, a larger storage modulus. For instance, Yang *et al.*[392] prepared GMRMs by **partial replacement** of CIP with Ni-coated multi-walled CNTs. **Dimorphic** GMRMs were prepared by Yu *et al.*[393] (using iron nanowires) and Yang *et al.*[394] (using flower-like CIP). Other exotic bidisperse GMRMs have been reported by dispersing PTFE particles together with CIP in an organogel to improve frictional properties.[395]

4.2. Plastomers

A promising GMRM in the borderline between MRFs and MREs is that of **MR plastomers (MRPs)** developed by Xinglong Gong and coworkers. For a recent **review on MRPs** we refer to Xuan *et al.*[396]

Liu *et al.*[397] investigated quasi-static loading rates (in particular, **start-up tests**). The **non-linear properties** of MRPs were investigated by Gong *et al.*[398] using torsional rheometry. Similar to Liao *et al.*[323] for MREs, **normal stresses** have also been investigated in MRPs.[399] They observed an abrupt drop in the normal stress of MRPs at high fields (>491 mT) and explained it in terms of sliding. Xu *et al.*[400] investigated **compressive, tensile and oscillatory squeeze** behaviors under constant volume. Three regions were distinguished in both compressive and tensile deformation modes: elastic deformation region, stress relaxation region and plastic flow region. Bidisperse MRPs have also been investigated in the literature. For instance, **carbon filler-doped MRPs** were synthesized by Xu *et al.*[401] More recently, Xu *et al.*[402] investigated the **dynamic compression properties** of MRPs in a modified Slit Hopkinson Pressure Bar (SHPB) device. A rate dependent stiffening performance was observed.

4.3. Other MR materials

Currently, many other MR materials exist apart from MRFs, MREs and GMRMs. Some examples are foamed MRE, impregnated MR composites and hybrid MRF-E materials.

Foamed MREs are porous MREs with cells being either open or close. Major advantages are a lighter weight and also the fact that the elasticity in the off-state can be tuned changing the porosity; it typically decreases with increasing porosity. They exhibit excellent vibration and acoustic absorption performance and can be used as sensors and actuators.[17] The storage modulus reduced and the loss factor increased when increasing the porosity. Stiffness and damping properties were easily controlled. Ju *et al.*[403] fabricated a foamed silicone-based

 This journal is © The Royal Society of Chemistry 2020

Open Access Article. Published on 01 September 2020. Downloaded on 2/15/2026 12:16:02 AM.
This article is licensed under a Creative Commons Attribution 3.0 Unported Licence.

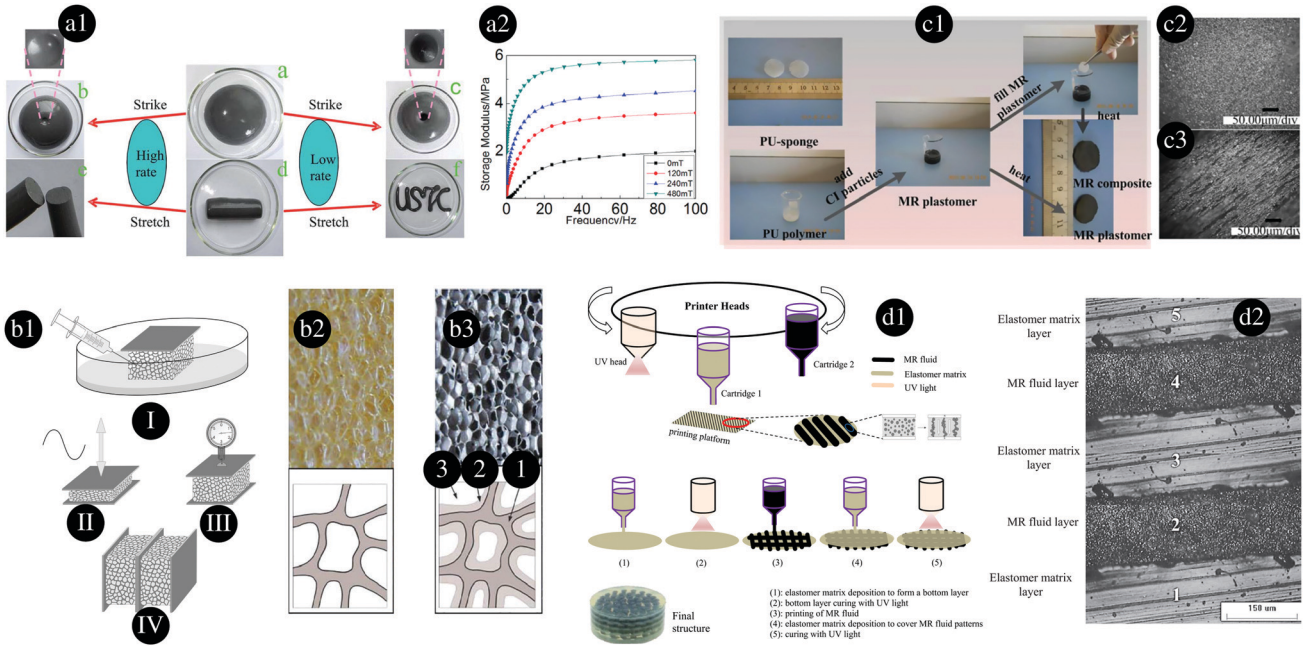

Fig. 6 (a1) Example of a GMRM consisting in CIP dispersed in a polymer matrix (silly putty) at 60 wt%. In the off-state, the GMRM exhibits the usual properties of the matrix, that is, it behaves as a brittle/soft material at large/small shear rates. (a2) Frequency dependence of the storage modulus of the GMRM shown in (a1) under different magnetic fields. The frequency to pass from soft to brittle material depends on the applied magnetic field. Adapted from Fig. 5 and 10 in ref. 383 with permission from RSC, copyright 2020. (b1) Manufacture process for an MRF impregnated polyurethane sponge. (I) Injection and immersion. (II) Oscillatory compression to guarantee homogeneous distribution of the MRF in the sponge. (III) Final MRF content is known by weighting. (IV) Joint of two specimens to perform oscillatory shear experiments (outer plates are fixed while a force/displacement is imposed in the inner one). (b2 and b3) Pictures of the polyurethane sponge without and with MRF, respectively. Inner sketch: (1) porous sponge, (2) layer of MRF, (3) empty space. Adapted from Fig. 3 and 4 in ref. 411 with permission from Elsevier, copyright 2020. (c1) Synthesis of a polyurethane sponge impregnated by a MRP. (c2 and c3) Particle disposition in the off- and on-state, respectively. As it can be seen, this composite allows particle motion as MRFs. Adapted from Fig. 2 in ref. 409 with permission from IOP Publishing, copyright 2020. (d1) Manufacture process to synthesize a hybrid material based on MRFs and a UV-curable elastomer. (d2) Cross-sectional picture of the resultant material. Adapted from Fig. 6 and 7 in ref. 418 with permission from Elsevier, copyright 2020.

MRE using ammonium bicarbonate. More recently, Plachy *et al.*[404] reported the synthesis of a foamed MRE using ethylene propylene diene rubber and azodicarbonamide as foaming agent.

Most **MRF impregnated composites** are based on **sponges** that serve as a scaffold for the MRF to be held in place due to capillary forces.[405,406] Examples on how to synthesize these composites are shown in Fig. 6b and c. The sponge is capable to withstand a certain stress and provides the desired viscoelastic properties. In a MRF impregnated sponge the particles within the MRF have some freedom to move around a sponge scaffold and this maximizes the MR effect. Most MRF impregnated sponges reported in the recent literature are based on polyurethane with open cell matrices.[407–411] An exception is the paper by Reddy *et al.*[412] that used a CNT foam.

Another set of MRF impregnated composites uses a **metal foam** as a skeleton. They were discovered with the aim to improve the mechanical strength over that of MRF impregnated sponges. Liu *et al.*[413] described the dynamic response of different metal foam MRF materials. They used three types of metal foams: Fe, Ni and Cu. They exhibit some advantages over the sponge MR materials: more wearable, longer lifetime and better damping effect. Yao *et al.*[414] investigated the normal force generated in metal foams subjected to oscillatory shear.

Finally, **hybrid MRF-E materials** share the benefits of MRFs and MREs as both MRFs and MREs coexist in the same composite structure. In fact, hybrid MREs can be fabricated by encapsulating a MRF within a UV-curable silicone elastomer[415–417] as it is shown in Fig. 6d. The elastic properties are provided by the MRE component while the damping properties are provided by the MRF component.

5. Conclusions and future trends

Currently, magnetorheology is a consolidated multidisciplinary field of research combining classical electromagnetism, fluid physics, mechanics and materials science. The MR family is growing fast and a number of potential applications are in development.

As described above, during the last ten years, the emphasis has been focused on designing materials that result in a stronger MR response and a better stability. This includes the synthesis of **core–shell magnetic particles** and preparation of **bidisperse MR composites**. Nevertheless, there is still plenty of room for improvement with new trends and challenges.

Probably, the most direct route to enhance MR effect is **maximizing the particle content**. In this sense, the use of new

Open Access Article. Published on 01 September 2020. Downloaded on 2/15/2026 12:16:02 AM.
This article is licensed under a Creative Commons Attribution 3.0 Unported Licence.

additives such as superplasticizers was found to be of interest, particularly in low field applications. Unfortunately, the technology has been developed for water based MRFs and it seems difficult to translate it to oil-based material applications.

Other alternatives involve the use of unconventional flow/magnetic field configurations. **Non-shearing (elongational) flows** are vaguely understood in the literature. Moreover, it is expected that **combined kinematics (*i.e.* superimposed flows)** will generate stronger responses. Similarly, cases where a DC magnetic field is used have been widely studied. However, by employing **triaxial unsteady magnetic fields**, it is possible to generate self-assembled structures that are closer to the minimum energy configuration. This could be useful in the fabrication of more efficient MRFs and MREs. In addition, it should be taken into consideration that the understanding of magnetorheology in **high speed and high magnetic fields** is still in its infancy.

Regarding stability, new research has given rise to a wide variety of **GMRMs** but their fundamental understanding is far to be complete. Only time independent matrices, and in particular **yield stress** materials, have been explored in detail to date although their viscoelastic properties have yet to receive enough attention. In any case, before attempting the previous goal, it seems reasonable to deepen in the understanding of **time dependent properties** of simpler MR composites that are still vaguely understood.[419,420] Even more difficult seems to be the understanding of **aging effects** in MR devices[421] due to the large difference between time/space scales between current applications and academia investigations.

Recent progress has led to improving MR applications from different perspectives. A few of these improvements include **IMREs together with AMREs in parallel and series configurations** when isotropic stiffness and damping characteristics are required, **mechanically deformable phases** in springless damping applications[422,423] or **electromagnetic and permanent magnetic assemblies** to reduce power consumption in applications where the MR composite operates frequently in the on-state.

Finally, it is anticipated that MR materials will be incorporated in applications related to **thermal transport and heat dissipation**[424,425] as well as within the context of other disciplines such as Ecology (for the removal of phosphorous and lake restoration),[426] **Biomedicine** (for the fabrication of magnetic scaffolds and tissue engineering)[427] or **Electronics** (for the fabrication of MR ionogels).[428]

Conflicts of interest

There are no conflicts to declare.

Acknowledgements

Matthew Terkel is acknowledged for improving the use of English in the manuscript. This work was supported by MICINN PID2019-104883GB-I00 project, Junta de Andalucía P18-FR-2465 project and European Regional Development Fund (ERDF). J. R. Morillas acknowledges FPU14/01576 fellowship.

References

1 M. R. Jolly, J. D. Carlson and B. C. Muñoz, *Smart Mater. Struct.*, 1996, **5**(5), 607.
2 J. Rabinow, *AIEE Trans.*, 1948, **67**, 1308–1315.
3 Y. Xu, X. Gong, S. Xuan, W. Zhang and Y. Fan, *Soft Matter*, 2011, **7**(11), 5246–5254.
4 R. Ahamed, S. B. Choi and M. M. Ferdaus, *J. Intell. Mater. Syst. Struct.*, 2018, **29**(10), 2051–2095.
5 R. M. Andrade, A. Bento Filho, C. B. S. Vimieiro and M. Pinotti, *Smart Mater. Struct.*, 2018, **27**(10), 105031.
6 J. W. Swan, J. L. Bauer, Y. Liu and E. M. Furst, *Soft Matter*, 2014, **10**(8), 1102–1109.
7 J. P. Segovia-Gutiérrez, J. de Vicente, A. M. Puertas and R. Hidalgo-Álvarez, *Phys. Rev. E*, 2017, **95**(5), 052601.
8 P. J. Rankin, J. M. Ginder and D. J. Klingenberg, *Curr. Opin. Colloid Interface Sci.*, 1998, **3**(4), 373–381.
9 D. J. Klingenberg, *AIChE J.*, 2001, **47**(2), 246–249.
10 G. Bossis, O. Volkova, S. Lācis and A. Meunier, in *Ferrofluids*, ed. S. Odenbach, Springer-Verlag, Berlin Heidelberg, 2002, vol. 11, pp. 202–230.
11 I. Bica, *J. Ind. Eng. Chem.*, 2006, **12**(4), 501–515.
12 F. D. Goncalves, J. H. Koo and M. Ahmadian, *Shock Vib. Dig.*, 2006, **38**(3), 203–220.
13 B. J. Park, F. F. Fang and H. J. Choi, *Soft Matter*, 2010, **6**(21), 5246–5253.
14 J. de Vicente, D. J. Klingenberg and R. Hidalgo-Álvarez, *Soft Matter*, 2011, **7**(8), 3701–3710.
15 Y. Li, J. Li, W. Li and H. Du, *Smart Mater. Struct.*, 2014, **23**(12), 123001.
16 A. Ghaffari, S. H. Hashemabadi and M. Ashtiani, *J. Intell. Mater. Syst. Struct.*, 2015, **26**(8), 881–904.
17 Ubaidillah, J. Sutrisno, A. Purwanto and S. A. Mazlan, *Adv. Eng. Mater.*, 2015, **17**(5), 563–597.
18 L. J. Felicia, S. Vinod and J. Philip, *J. Nanofluids*, 2016, **5**(1), 1–22.
19 M. A. Cantera, M. Behrooz, R. F. Gibson and F. Gordaninejad, *Smart Mater. Struct.*, 2017, **26**(2), 023001.
20 S. B. Choi and Y. M. Han, *Magnetorheological fluid technology: applications in vehicle systems*, CRC Press, Boca Raton, 2012.
21 N. M. Wereley, *Magnetorheology: Advances and Applications*, Royal Society of Chemistry: RSC Smart Materials, London, 2013.
22 A. Hajalilou, S. A. Mazlan, H. Lavvafi and K. Shameli, *Field responsive fluids as smart materials*, Springer, Singapore, 2016.
23 S. B. Choi and W. Li, *Magnetorheological Materials and their Applications*, The Institution of Engineering and Technology, Stevenage, 2019.
24 S. Singamaneni, V. N. Bliznyuk, C. Binek and E. Y. Tsymbal, *J. Mater. Chem.*, 2011, **21**(42), 16819–16845.

This journal is © The Royal Society of Chemistry 2020

Open Access Article. Published on 01 September 2020. Downloaded on 2/15/2026 12:16:02 AM.
This article is licensed under a Creative Commons Attribution 3.0 Unported Licence.

25 H. S. Chae, S. H. Piao and H. J. Choi, *J. Ind. Eng. Chem.*, 2015, **29**, 129–133.
26 A. V. Anupama, V. Kumaran and B. Sahoo, *Powder Technol.*, 2018, **338**, 190–196.
27 Y. Tong, X. Dong and M. Qi, *Soft Matter*, 2018, **14**(18), 3504–3509.
28 W. Zhang, F. Shen and R. Hong, *Particuology*, 2011, **9**(2), 179–186.
29 Z. Kozakova, I. Kuritka, N. E. Kazantseva, V. Babayan, M. Pastorek, M. Machovsky, P. Bazant and P. Sáha, *Dalton Trans.*, 2015, **44**(48), 21099–21108.
30 L. Zhuang, W. Zhang, Y. Zhao, H. Shen, H. Lin and J. Liang, *Sci. Rep.*, 2015, **5**, 9320.
31 H. S. Jung and H. J. Choi, *J. Appl. Phys.*, 2015, **117**(17), 17E708.
32 L. Pei, H. Pang, K. Chen, S. Xuan and X. Gong, *Soft Matter*, 2018, **14**(24), 5080–5091.
33 J. Berasategi, A. Gómez, M. M. Bou-Ali, J. Gutiérrez, J. M. Barandiarán, I. V. Beketov, A. P. Safronov and G. V. Kurlyandskaya, *Smart Mater. Struct.*, 2018, **27**(4), 045011.
34 J. Noma, H. Abe, T. Kikuchi, J. Furusho and M. Naito, *J. Magn. Magn. Mater.*, 2010, **322**(13), 1868–1871.
35 I. Arief and P. K. Mukhopadhyay, *J. Magn. Magn. Mater.*, 2016, **397**, 57–63.
36 I. Arief and P. K. Mukhopadhyay, *J. Magn. Magn. Mater.*, 2019, **479**, 326–331.
37 Z. Xia, X. Wu, G. Peng, L. Wang, W. Li and W. Wen, *Smart Mater. Struct.*, 2017, **26**(5), 054006.
38 Z. Xia and W. Wen, *Nanomaterials*, 2016, **6**(1), 19.
39 J. Rodríguez-López, H. C. Shum, L. Elvira, F. Montero de Espinosa and D. A. Weitz, *J. Magn. Magn. Mater.*, 2013, **326**, 220–224.
40 M. W. Kim, D. H. Bae, S. H. Kwon and H. J. Choi, *Macromol. Res.*, 2018, **26**(4), 353–358.
41 S. Lee, K. Y. Shin and J. Jang, *Nanoscale*, 2015, **7**(21), 9646–9654.
42 M. Sedlačík, V. Pavlínek, M. Lehocky, A. Mracek, O. Grulich, P. Švrčinová, P. Filip and A. Vesel, *Colloids Surf., A*, 2011, **387**(1–3), 99–103.
43 M. Sedlačík, V. Pavlínek, P. Sáha, P. Švrčinová and P. Filip, *Mod. Phys. Lett. B*, 2012, **26**(03), 1150013.
44 H. B. Cheng, L. Zuo, J. H. Song, Q. J. Zhang and N. M. Wereley, *J. Appl. Phys.*, 2010, **107**(9), 09B507.
45 H. Cheng, M. Wang, C. Liu and N. M. Wereley, *Smart Mater. Struct.*, 2018, **27**(7), 075030.
46 M. Ashtiani, S. H. Hashemabadi and A. Ghaffari, *J. Magn. Magn. Mater.*, 2015, **374**, 716–730.
47 Y. P. Seo, S. Han, J. Choi, A. Takahara, H. J. Choi and Y. Seo, *Adv. Mater.*, 2018, **30**(42), 1704769.
48 M. Ashtiani and S. H. Hashemabadi, *Colloids Surf., A*, 2015, **469**, 29–35.
49 G. Bossis, Y. Grasselli, A. Meunier and O. Volkova, *Appl. Phys. Lett.*, 2016, **109**(11), 111902.
50 T. Plachý, E. Kutalkova, M. Sedlačík, A. Vesel, M. Masar and I. Kuritka, *J. Ind. Eng. Chem.*, 2018, **66**, 362–369.
51 Y. M. Han, S. Kim, Y. D. Park, J. W. Kang and S. B. Choi, *Smart Mater. Struct.*, 2015, **24**(11), 115016.
52 J. F. Desrosiers, J. P. Lucking Bigué, M. Denninger, G. Julió, J. S. Plante and F. Charron, *J. Phys.: Conf. Ser.*, 2013, **412**(1), 012022.
53 A. Wiehe, C. Kieburg and J. Maas, *J. Phys.: Conf. Ser.*, 2013, **412**(1), 012017.
54 J. P. Lucking Bigué, A. Landry-Blais, A. Pin, R. Pilon, J. S. Plante, X. Chen and M. Andrews, *Smart Mater. Struct.*, 2019, **28**(9), 094003.
55 S. A. Wahid, I. Ismail, S. Aid and M. S. A. Rahim, *IOP Conf. Ser.: Mater. Sci. Eng.*, 2016, **114**(1), 012101.
56 C. Kieburg, G. Oetter, R. Lochtman, C. Gabriel, H. M. Laun, J. Pfister, G. Schober and H. Steinwender, in *Proc. 10th Intl. Conf. on Electrorheological Fluids and Magneto-rheological Suspensions*, World Scientific, Singapore, 2007, pp. 101–107.
57 J. R. Morillas, A. J. F. Bombard and J. de Vicente, *Smart Mater. Struct.*, 2015, **25**(1), 015023.
58 F. H. Niu, Z. D. Hu, H. Yan, J. J. Yang and H. S. Zhang, *J. Magn. Magn. Mater.*, 2018, **465**, 421–429.
59 H. Cheng, X. Zhang, G. Liu, W. Ma and N. M. Wereley, *Smart Mater. Struct.*, 2016, **25**(5), 055007.
60 S. R. Gorodkin, W. I. Kordonski, E. V. Medvedeva, Z. A. Novikova, A. B. Shorey and S. D. Jacobs, *Rev. Sci. Instrum.*, 2000, **71**(6), 2476–2480.
61 W. I. Kordonski, S. Gorodkin and R. Behlok, *J. Magn. Magn. Mater.*, 2015, **382**, 328–334.
62 J. Roupec, P. Berka, I. Mazůrek, Z. Strecker, M. Kubík, O. Macháček and M. T. Andani, *Smart Mater. Struct.*, 2017, **26**(10), 107001.
63 L. Xie, Y. T. Choi, C. R. Liao and N. M. Wereley, *J. Appl. Phys.*, 2015, **117**(17), 17C754.
64 Y. T. Choi, L. Xie and N. M. Wereley, *Smart Mater. Struct.*, 2016, **25**(4), 04LT01.
65 M. Wen, J. Chambers, S. G. Sherman and N. M. Wereley, *Smart Mater. Struct.*, 2019, **28**(2), 025039.
66 Y. D. Liu, F. F. Fang and H. J. Choi, *Colloid Polym. Sci.*, 2011, **289**(11), 1295–1298.
67 C. Y. Gao, M. W. Kim, D. H. Bae, Y. Z. Dong, S. H. Piao and H. J. Choi, *Polymer*, 2017, **125**, 21–29.
68 M. Sedlačík, V. Pavlínek, P. Sáha, P. Švrčinová, P. Filip and J. Stejskal, *Smart Mater. Struct.*, 2010, **19**(11), 115008.
69 M. Cvek, M. Mrlík, M. Ilčíková, T. Plachý, M. Sedlačík, J. Mosnáček and V. Pavlínek, *J. Mater. Chem. C*, 2015, **3**(18), 4646–4656.
70 M. Mrlík, M. Ilčíková, V. Pavlínek, J. Mosnáček, P. Peer and P. Filip, *J. Colloid Interface Sci.*, 2013, **396**, 146–151.
71 J. W. Lee, K. P. Hong, M. W. Cho, S. H. Kwon and H. J. Choi, *Smart Mater. Struct.*, 2015, **24**(6), 065002.
72 A. Esmaeilzare, S. M. Rezaei and B. Ramezanzadeh, *Appl. Surf. Sci.*, 2018, **436**, 1200–1212.
73 B. Sim, H. S. Chae and H. J. Choi, *eXPRESS Polym. Lett.*, 2015, **9**(8), 736–743.
74 T. H. Min, H. J. Choi, N. H. Kim, K. Park and C. Y. You, *Colloids Surf., A*, 2017, **531**, 48–55.
75 K. Chen, W. L. Zhang, L. Shan, X. Zhang, Y. Meng, H. J. Choi and Y. Tian, *J. Appl. Phys.*, 2014, **116**(15), 153508.

Open Access Article. Published on 01 September 2020. Downloaded on 2/15/2026 12:16:02 AM. This article is licensed under a Creative Commons Attribution 3.0 Unported Licence.

76 Y. D. Liu, C. H. Hong and H. J. Choi, *Macromol. Res.*, 2012, **20**(12), 1211–1218.
77 Y. Z. Dong, S. H. Piao and H. J. Choi, *Colloid Polym. Sci.*, 2018, **296**(1), 11–19.
78 A. Hajalilou, A. Kianvash, K. Shameli and H. Lavvafi, *Appl. Phys. Lett.*, 2017, **110**(26), 261902.
79 G. Kim, J. E. Kim, Y. D. Liu and H. J. Choi, *IEEE Trans. Magn.*, 2012, **48**(11), 3446–3449.
80 S. Y. Kim, S. H. Kwon, Y. D. Liu, J. S. Lee, C. Y. You and H. J. Choi, *J. Mater. Sci.*, 2014, **49**(3), 1345–1352.
81 S. H. Kwon, H. J. Choi, J. W. Lee, K. P. Hong and M. W. Cho, *J. Korean Phys. Soc.*, 2013, **62**(12), 2118–2122.
82 S. H. Kwon, B. Sim and H. J. Choi, *IEEE Trans. Magn.*, 2016, **52**(7), 1–4.
83 P. B. Nguyen, X. P. Do, J. Jeon, S. B. Choi, Y. D. Liu and H. J. Choi, *J. Magn. Magn. Mater.*, 2014, **367**, 69–74.
84 B. O. Park, K. H. Song, B. J. Park and H. J. Choi, *J. Appl. Phys.*, 2010, **107**(9), 09A506.
85 D. E. Park, H. S. Chae, H. J. Choi and A. Maity, *J. Mater. Chem. C*, 2015, **3**(13), 3150–3158.
86 S. H. Piao, M. Bhaumik, A. Maity and H. J. Choi, *J. Mater. Chem. C*, 2015, **3**(8), 1861–1868.
87 H. S. Chae, S. H. Piao, W. J. Han and H. J. Choi, *Macromol. Chem. Phys.*, 2018, **219**(5), 1700408.
88 F. F. Fang and H. J. Choi, *Colloid Polym. Sci.*, 2010, **288**(1), 79–84.
89 F. F. Fang, H. J. Choi and W. S. Choi, *Colloid Polym. Sci.*, 2010, **288**(3), 359–363.
90 F. F. Fang, H. J. Choi and Y. Seo, *ACS Appl. Mater. Interfaces*, 2010, **2**(1), 54–60.
91 Y. D. Liu, H. J. Choi and S. B. Choi, *Colloids Surf., A*, 2012, **403**, 133–138.
92 Y. D. Liu and H. J. Choi, *J. Appl. Phys.*, 2014, **115**(17), 17B529.
93 Y. D. Liu and H. J. Choi, *Mater. Res. Bull.*, 2015, **69**, 92–97.
94 L. Pei, H. Pang, X. Ruan, X. Gong and S. Xuan, *RSC Adv.*, 2017, **7**(14), 8142–8150.
95 M. H. Kim, K. Choi, J. D. Nam and H. J. Choi, *Smart Mater. Struct.*, 2017, **26**(9), 095006.
96 K. H. Gudmundsson, F. Jonsdottir, F. Thorsteinsson and O. Gutfleisch, *J. Intell. Mater. Syst. Struct.*, 2011, **22**(15), 1763–1767.
97 W. Jiang, Y. Zhang, S. Xuan, C. Guo and X. Gong, *J. Magn. Magn. Mater.*, 2011, **323**(24), 3246–3250.
98 L. A. Powell, N. M. Wereley and J. C. Ulicny, *IEEE Trans. Magn.*, 2012, **48**(11), 3764–3767.
99 L. M. Armijo, L. A. Ahuré-Powell and N. M. Wereley, *J. Appl. Phys.*, 2015, **117**(17), 17C747.
100 M. Ashtiani and S. H. Hashemabadi, *J. Intell. Mater. Syst. Struct.*, 2015, **26**(14), 1887–1892.
101 I. Arief and P. K. Mukhopadhyay, *J. Alloys Compd.*, 2017, **696**, 1053–1058.
102 D. Kittipoomwong, D. J. Klingenberg and J. C. Ulicny, *J. Rheol.*, 2005, **49**(6), 1521–1538.
103 C. Ekwebelam and H. See, *Rheol. Acta*, 2009, **48**(1), 19–32.
104 N. M. Wereley, A. Chaudhuri, J. H. Yoo, S. John, S. Kotha, A. Suggs, R. Radhakrishnan, B. J. Love and T. S. Sudarshan, *J. Intell. Mater. Syst. Struct.*, 2006, **17**(5), 393–401.
105 C. Magnet, P. Kuzhir, G. Bossis, A. Meunier, L. Suloeva and A. Zubarev, *Phys. Rev. E: Stat., Nonlinear, Soft Matter Phys.*, 2012, **86**(1), 011404.
106 J. R. Morillas, A. J. F. Bombard and J. de Vicente, *Smart Mater. Struct.*, 2018, **27**(7), 07LT01.
107 M. Sedlačík, V. Pavlínek, R. Vyroubal, P. Peer and P. Filip, *Smart Mater. Struct.*, 2013, **22**(3), 035011.
108 A. J. F. Bombard, F. R. Gonçalves, J. R. Morillas and J. de Vicente, *Smart Mater. Struct.*, 2014, **23**(12), 125013.
109 J. R. Morillas, A. J. F. Bombard and J. de Vicente, *Ind. Eng. Chem. Res.*, 2018, **57**(40), 13427–13436.
110 I. Arief and P. K. Mukhopadhyay, *Phys. B*, 2014, **448**, 73–76.
111 E. Esmaeilnezhad, H. J. Choi, M. Schaffie, M. Gholizadeh, M. Ranjbar and S. H. Kwon, *J. Magn. Magn. Mater.*, 2017, **444**, 161–167.
112 D. S. Jang, Y. D. Liu, J. H. Kim and H. J. Choi, *Colloid Polym. Sci.*, 2015, **293**(2), 641–647.
113 I. Jönkkäri, M. Sorvali, H. Huhtinen, E. Sarlin, T. Salminen, J. Haapanen, J. M. Mäkelä and J. Vuorinen, *Smart Mater. Struct.*, 2017, **26**(9), 095004.
114 D. J. Klingenberg and J. C. Ulicny, *Int. J. Mod. Phys. B*, 2011, **25**(07), 911–917.
115 S. A. N. Leong, P. M. Samin, A. Idris, S. A. Mazlan and A. H. A. Rahman, *Smart Mater. Struct.*, 2016, **25**(2), 025025.
116 J. A. Marins, T. Plachý and P. Kuzhir, *J. Rheol.*, 2019, **63**(1), 125–139.
117 D. Susan-Resiga and L. Vékás, *Rheol. Acta*, 2014, **53**(8), 645–653.
118 D. Susan-Resiga and L. Vékás, *J. Rheol.*, 2017, **61**(3), 401–408.
119 D. Susan-Resiga and P. Barvinschi, *J. Rheol.*, 2018, **62**(3), 739–752.
120 S. H. Piao, W. L. Zhang and H. J. Choi, *IEEE Trans. Magn.*, 2013, **50**(1), 1–4.
121 H. S. Chae, S. H. Piao, A. Maity and H. J. Choi, *Colloid Polym. Sci.*, 2015, **293**(1), 89–95.
122 M. Cvek, M. Mrlík, R. Moucka and M. Sedlačík, *Colloids Surf., A*, 2018, **543**, 83–92.
123 S. H. Kwon, C. H. Hong, P. X. Do, S. B. Choi and H. J. Choi, *Ind. Eng. Chem. Res.*, 2015, **54**(16), 4655–4663.
124 F. Jonsdottir, K. H. Gudmundsson, T. B. Dijkman, F. Thorsteinsson and O. Gutfleisch, *J. Intell. Mater. Syst. Struct.*, 2010, **21**(11), 1051–1060.
125 G. T. Ngatu, N. M. Wereley, J. O. Karli and R. C. Bell, *Smart Mater. Struct.*, 2008, **17**(4), 045022.
126 A. J. F. Bombard and J. V. R. Teodoro, *Int. J. Mod. Phys. B*, 2011, **25**(07), 943–946.
127 P. Domínguez-García, S. Melle, J. M. Pastor and M. A. Rubio, *Phys. Rev. E: Stat., Nonlinear, Soft Matter Phys.*, 2007, **76**(5), 051403.
128 K. Shahrivar, E. Carreón-González, J. R. Morillas and J. de Vicente, *Soft Matter*, 2017, **13**(14), 2677–2685.
129 G. I. Vega-Bellido, R. A. de la Cruz-Araujo, I. Kretzschmar and U. M. Córdova-Figueroa, *Soft Matter*, 2019, **15**(20), 4078–4086.
130 T. Borbáth, I. Borbáth, S. Günther, O. Marinica, L. Vékás and S. Odenbach, *Smart Mater. Struct.*, 2014, **23**(5), 055018.

 This journal is © The Royal Society of Chemistry 2020

Open Access Article. Published on 01 September 2020. Downloaded on 2/15/2026 12:16:02 AM. This article is licensed under a Creative Commons Attribution 3.0 Unported Licence.

131 C. L. Berli and J. de Vicente, *Appl. Phys. Lett.*, 2012, **101**(2), 021903.
132 H. M. Laun, G. Schmidt, C. Gabriel and C. Kieburg, *Rheol. Acta*, 2008, **47**(9), 1049–1059.
133 W. Hu and N. M. Wereley, *Int. J. Mod. Phys. B*, 2011, **25**, 979–985.
134 D. Güth and J. Maas, *J. Intell. Mater. Syst. Struct.*, 2016, **27**(5), 689–704.
135 P. Kuzhir, C. Magnet, L. Rodríguez-Arco, M. T. López-López, H. Fezai, A. Meunier, A. Zubarev and G. Bossis, *J. Rheol.*, 2014, **58**(6), 1829–1853.
136 H. M. Laun, C. Gabriel and C. Kieburg, *Rheol. Acta*, 2011, **50**(2), 141–157.
137 I. Jönkkäri, E. Kostamo, J. Kostamo, S. Syrjala and M. Pietola, *Smart Mater. Struct.*, 2012, **21**(7), 075030.
138 J. R. Morillas and J. de Vicente, *Composites, Part B*, 2019, **160**, 626–631.
139 C. W. Guo, F. Chen, Q. R. Meng and Z. X. Dong, *J. Magn. Magn. Mater.*, 2014, **360**, 174–177.
140 M. Cvek, M. Mrlík and V. Pavlínek, *J. Rheol.*, 2016, **60**(4), 687–694.
141 S. G. Sherman, A. C. Becnel and N. M. Wereley, *J. Magn. Magn. Mater.*, 2015, **380**, 98–104.
142 J. A. Ruiz-López, J. C. Fernández-Toledano, R. Hidalgo-Álvarez and J. de Vicente, *Soft Matter*, 2016, **12**(5), 1468–1476.
143 J. A. Ruiz-López, R. Hidalgo-Álvarez and J. de Vicente, *Smart Mater. Struct.*, 2017, **26**(5), 054001.
144 W. Jia, L. Shan, W. Zhang, Y. Meng and Y. Tian, *Smart Mater. Struct.*, 2018, **27**(10), 105019.
145 Y. Sakuda, M. Aoshima and A. Satoh, *Mol. Phys.*, 2012, **110**(13), 1429–1435.
146 J. M. Ginder and L. C. Davis, *Appl. Phys. Lett.*, 1994, **65**(26), 3410–3412.
147 H. M. Laun, C. Gabriel and C. Kieburg, *J. Rheol.*, 2010, **54**(2), 327–354.
148 M. Ocalan and G. H. McKinley, *Rheol. Acta*, 2013, **52**(7), 623–641.
149 J. R. Morillas, J. Yang and J. de Vicente, *J. Rheol.*, 2018, **62**(6), 1485–1494.
150 G. Bossis, O. Volkova, Y. Grasselli and A. Ciffreo, *Front. Mater.*, 2019, **6**, 4.
151 J. R. Morillas and J. de Vicente, *Soft Matter*, 2019, **15**(16), 3330–3342.
152 J. R. Morillas and J. de Vicente, *Phys. Rev. E*, 2019, **99**(6), 062604.
153 J. Wu, L. Pei, S. Xuan, Q. Yan and X. Gong, *J. Magn. Magn. Mater.*, 2016, **408**, 18–25.
154 K. Shahrivar, J. R. Morillas, Y. Luengo, H. Gavilan, P. Morales, C. Bierwisch and J. de Vicente, *J. Rheol.*, 2019, **63**(4), 547–558.
155 R. C. Bell, J. O. Karli, A. N. Vavreck, D. T. Zimmerman, G. T. Ngatu and N. M. Wereley, *Smart Mater. Struct.*, 2008, **17**(1), 015028.
156 J. de Vicente, J. P. Segovia-Gutiérrez, E. Andablo-Reyes, F. Vereda and R. Hidalgo-Álvarez, *J. Chem. Phys.*, 2009, **131**(19), 194902.
157 J. de Vicente, F. Vereda, J. P. Segovia-Gutiérrez, M. del Puerto Morales and R. Hidalgo-Álvarez, *J. Rheol.*, 2010, **54**(6), 1337–1362.
158 A. Gómez-Ramírez, P. Kuzhir, M. T. López-López, G. Bossis, A. Meunier and J. D. G. Durán, *J. Rheol.*, 2011, **55**(1), 43–67.
159 J. R. Morillas, E. Carreón-González and J. de Vicente, *Smart Mater. Struct.*, 2015, **24**(12), 125005.
160 K. Shah and S. B. Choi, *Smart Mater. Struct.*, 2014, **24**(1), 015004.
161 P. Kuzhir, A. Gómez-Ramírez, M. T. López-López, G. Bossis and A. Zubarev, *J. Non-Newtonian Fluid Mech.*, 2011, **166**(7–8), 373–385.
162 G. Bossis, J. A. Marins, P. Kuzhir, O. Volkova and A. Zubarev, *J. Intell. Mater. Syst. Struct.*, 2015, **26**(14), 1871–1879.
163 J. de Vicente, F. González-Caballero, G. Bossis and O. Volkova, *J. Rheol.*, 2002, **46**(5), 1295–1303.
164 Y. T. Chan, P. Wong, K. P. Liu and W. Bullough, *J. Intell. Mater. Syst. Struct.*, 2011, **22**(6), 551–560.
165 J. Jiang, Y. Tian, D. Ren and Y. Meng, *Smart Mater. Struct.*, 2011, **20**(8), 085012.
166 X. Liu, D. Ye, X. Gao, F. Li, M. Sun, H. Zhang, T. Tu and H. Yu, *J. Magn. Magn. Mater.*, 2016, **398**, 137–140.
167 X. Y. Yao, M. Yu and J. Fu, *Smart Mater. Struct.*, 2015, **24**(3), 035001.
168 C. Guo, X. Gong, S. Xuan, L. Zong and C. Peng, *J. Magn. Magn. Mater.*, 2012, **324**(6), 1218–1224.
169 G. Yildirim and S. Genç, *Smart Mater. Struct.*, 2013, **22**(8), 085001.
170 S. G. Sherman, L. A. Powell, A. C. Becnel and N. M. Wereley, *J. Appl. Phys.*, 2015, **117**(17), 17C751.
171 D. M. Patel and R. V. Upadhyay, *Mater. Res. Express*, 2018, **6**(1), 015707.
172 X. Ruan, Y. Wang, S. Xuan and X. Gong, *Smart Mater. Struct.*, 2017, **26**(3), 035067.
173 A. G. Olabi and A. Grunwald, *Mater. Des.*, 2007, **28**(10), 2658–2664.
174 B. Kavlicoglu, F. Gordaninejad and X. Wang, *J. Appl. Mech.*, 2011, **78**(4), 041008.
175 H. Nishiyama, H. Takana, K. Shinohara, K. Mizuki, K. Katagiri and M. Ohta, *J. Magn. Magn. Mater.*, 2011, **323**(10), 1293–1297.
176 M. Kubík, O. Macháček, Z. Strecker, J. Roupec and I. Mazůrek, *Smart Mater. Struct.*, 2017, **26**(4), 047002.
177 G. Hu, J. Zhang, F. Zhong and L. Yu, *Smart Mater. Struct.*, 2019, **28**(4), 047003.
178 M. Kubik, D. Pavliček, O. Macháček, Z. Strecker and J. Roupec, *Smart Mater. Struct.*, 2019, **28**(4), 047002.
179 H. G. Lagger, C. Bierwisch and M. Moseler, *J. Phys.: Conf. Ser.*, 2013, **412**(1), 012020.
180 H. G. Lagger, C. Bierwisch, J. G. Korvink and M. Moseler, *Rheol. Acta*, 2014, **53**(5–6), 417–443.
181 H. G. Lagger, T. Breinlinger, J. G. Korvink, M. Moseler, A. Di Renzo, F. Di Maio and C. Bierwisch, *J. Non-Newtonian Fluid Mech.*, 2015, **218**, 16–26.

Open Access Article. Published on 01 September 2020. Downloaded on 2/15/2026 12:16:02 AM. This article is licensed under a Creative Commons Attribution 3.0 Unported Licence.

182 D. Vågberg and B. P. Tighe, *Soft Matter*, 2017, **13**(39), 7207–7221.
183 S. G. Sherman, D. A. Paley and N. M. Wereley, *IEEE Trans. Magn.*, 2012, **48**(11), 3517–3520.
184 S. G. Sherman and N. M. Wereley, *IEEE Trans. Magn.*, 2013, **49**(7), 3430–3433.
185 J. A. Ruiz-López, Z. W. Wang, J. C. Fernández-Toledano, R. Hidalgo-Álvarez and J. de Vicente, *Rheol. Acta*, 2016, **55**(3), 245–256.
186 D. J. Klingenberg, C. H. Olk, M. A. Golden and J. C. Ulicny, *J. Phys.: Condens. Matter*, 2010, **22**(32), 324101.
187 B. T. Wilson and D. J. Klingenberg, *J. Rheol.*, 2017, **61**(4), 601–611.
188 J. C. Ulicny, K. S. Snavely, M. A. Golden and D. J. Klingenberg, *Appl. Phys. Lett.*, 2010, **96**(23), 231903.
189 K. Okada and A. Satoh, *J. Magn. Magn. Mater.*, 2017, **437**, 29–41.
190 S. Zhang, J. Zhou and C. Shao, *Phys. Fluids*, 2019, **31**(2), 022005.
191 J. de Vicente, J. A. Ruiz-López, E. Andablo-Reyes, J. P. Segovia-Gutiérrez and R. Hidalgo-Álvarez, *J. Rheol.*, 2011, **55**(4), 753–779.
192 J. A. Ruiz-López, R. Hidalgo-Álvarez and J. de Vicente, *Rheol. Acta*, 2016, **55**(3), 215–221.
193 J. A. Ruiz-López, R. Hidalgo-Álvarez and J. de Vicente, *Rheol. Acta*, 2012, **51**(7), 595–602.
194 A. Farjoud, M. Ahmadian, N. Mahmoodi, X. Zhang and M. Craft, *Smart Mater. Struct.*, 2011, **20**(8), 085013.
195 W. Kordonski and S. Gorodkin, *J. Rheol.*, 2016, **60**(1), 129–139.
196 C. Guo, X. Gong, S. Xuan, Q. Yan and X. Ruan, *Smart Mater. Struct.*, 2013, **22**(4), 045020.
197 W. Horak, *Smart Mater. Struct.*, 2018, **27**(6), 065022.
198 I. Ismail, S. A. Mazlan, H. Zamzuri and A. G. Olabi, *Jpn. J. Appl. Phys.*, 2012, **51**(6R), 067301.
199 W. Horak, B. Sapiński and M. Szczęch, *Acta Mech. Autom.*, 2017, **11**(1), 64–68.
200 S. Kaluvan, K. Shah and S. B. Choi, *Smart Mater. Struct.*, 2014, **23**(11), 115017.
201 X. Tang, X. Zhang, R. Tao and Y. Rong, *J. Appl. Phys.*, 2000, **87**(5), 2634–2638.
202 C. Hegger and J. Maas, *J. Intell. Mater. Syst. Struct.*, 2016, **27**(14), 1895–1907.
203 J. P. Lucking Bigué, F. Charron and J. S. Plante, *J. Intell. Mater. Syst. Struct.*, 2018, **29**(1), 62–71.
204 J. P. Lucking Bigué, F. Charron and J. S. Plante, *J. Intell. Mater. Syst. Struct.*, 2018, **29**(1), 72–81.
205 R. H. Ewoldt, P. Tourkine, G. H. McKinley and A. E. Hosoi, *Phys. Fluids*, 2011, **23**(7), 073104.
206 S. H. Sadek, H. H. Najafabadi and F. J. Galindo-Rosales, *J. Rheol.*, 2020, **64**(1), 55–65.
207 F. J. Galindo-Rosales, J. P. Segovia-Gutiérrez, F. T. Pinho, M. A. Alves and J. de Vicente, *J. Rheol.*, 2015, **59**(1), 193–209.
208 H. Wang, C. Bi, J. Kan, C. Gao and W. Xiao, *J. Intell. Mater. Syst. Struct.*, 2011, **22**(8), 811–816.
209 S. Rahimi and D. Weihs, *Exp. Fluids*, 2012, **53**(5), 1577–1589.
210 A. K. El Wahed and C. A. McEwan, *J. Intell. Mater. Syst. Struct.*, 2011, **22**(7), 631–643.
211 M. Pichumani and W. González-Viñas, *Soft Matter*, 2013, **9**(8), 2506–2511.
212 P. Skalski and K. Kalita, *Acta Mech. Autom.*, 2017, **11**(4), 267–274.
213 X. Zhu, X. Jing and L. Cheng, *J. Intell. Mater. Syst. Struct.*, 2012, **23**(8), 839–873.
214 A. Y. Abd Fatah, S. A. Mazlan, T. Koga, H. Zamzuri, M. Zeinali and F. Imaduddin, *Int. J. Mod. Phys. B*, 2015, **29**(04), 1530004.
215 J. W. Sohn, G. W. Kim and S. B. Choi, *Appl. Sci.*, 2018, **8**(10), 1928.
216 W. H. Kim, J. H. Park, S. Kaluvan, Y. S. Lee and S. B. Choi, *Sens. Actuators, A*, 2017, **255**, 104–117.
217 T. H. Lee and S. B. Choi, *Smart Mater. Struct.*, 2018, **28**(1), 014001.
218 X. Gong, X. Ruan, S. Xuan, Q. Yan and H. Deng, *Adv. Mech. Eng.*, 2014, **6**, 410158.
219 B. Sapiński and J. Gołdasz, *Smart Mater. Struct.*, 2015, **24**(11), 115007.
220 J. Yang, S. Sun, W. Li, H. Du, G. Alici and M. Nakano, *J. Intell. Mater. Syst. Struct.*, 2015, **26**(14), 1811–1817.
221 S. R. Patil and R. A. Lohar, *J. Braz. Soc. Mech. Sci. Eng.*, 2018, **40**(11), 546.
222 J. Roupec, I. Mazůrek, Z. Strecker and M. Klapka, *J. Phys.: Conf. Ser.*, 2013, **412**(1), 012024.
223 J. D. Carlson, *J. Intell. Mater. Syst. Struct.*, 2002, **13**(7–8), 431–435.
224 J. D. Carlson, *Int. J. Vehicle Des.*, 2003, **33**(1–3), 207–217.
225 J. C. Ulicny, M. P. Balogh, N. M. Potter and R. A. Waldo, *Mater. Sci. Eng., A*, 2007, **443**(1–2), 16–24.
226 M. A. Bramantya, M. Motozawa and T. Sawada, *J. Phys.: Condens. Matter*, 2010, **22**(32), 324102.
227 M. A. Bramantya and T. Sawada, *J. Magn. Magn. Mater.*, 2011, **323**(10), 1330–1333.
228 A. Nanda and M. A. Karami, *J. Acoust. Soc. Am.*, 2018, **144**(1), 412–420.
229 Y. Forero-Sandoval, A. Vega-Flick, J. J. Alvarado-Gil and R. A. Medina-Esquivel, *Smart Mater. Struct.*, 2016, **26**(2), 025010.
230 M. S. A. Rahim, I. Ismail, S. B. Choi, W. H. Azmi and S. N. Aqida, *Smart Mater. Struct.*, 2017, **26**(11), 115009.
231 E. Esmaeilnezhad, S. Le Van, H. J. Choi, B. H. Chon, M. Schaffie, M. Gholizadeh and M. Ranjbar, *J. Environ. Manage.*, 2019, **231**, 1127–1134.
232 S. D. Nair and R. D. Ferron, *Rheol. Acta*, 2016, **55**(7), 571–579.
233 J. Ding, G. Peng, K. Shu, C. Wang, T. Tian, W. Yang, Y. Zhang, G. G. Wallace and W. Li, *Sci. Rep.*, 2015, **5**(1), 1–11.
234 Z. Chen, L. Ren, J. Li, L. Yao, Y. Chen, B. Liu and L. Jiang, *Acta Biomater.*, 2018, **65**, 283–291.
235 C. Hartzell, Y. T. Choi, N. M. Wereley and T. J. Leps, *Smart Mater. Struct.*, 2019, **28**, 035030.

 This journal is © The Royal Society of Chemistry 2020

Open Access Article. Published on 01 September 2020. Downloaded on 2/15/2026 12:16:02 AM. This article is licensed under a Creative Commons Attribution 3.0 Unported Licence.

236 Y. Zhang, D. Li, Y. Chen and Z. Li, *IEEE Trans. Magn.*, 2018, **54**(12), 1–7.
237 Y. Sato and S. Umebara, *IEEE Trans. Magn.*, 2012, **48**(11), 3521–3524.
238 V. A. Kuzmin, E. V. Korobko, V. P. Roizman, Z. A. Novikova, A. P. Dostanko and A. O. Karabko, *J. Phys.: Conf. Ser.*, 2013, **412**(1), 012021.
239 C. Majidi and R. J. Wood, *Appl. Phys. Lett.*, 2010, **97**(16), 164104.
240 P. H. Anjos, S. A. Lira and J. A. Miranda, *Phys. Rev. Fluids*, 2018, **3**(4), 044002.
241 A. M. Sidpara, *Opt. Eng.*, 2014, **53**(9), 092002.
242 N. A. Mutalib, I. Ismail, S. M. Soffie and S. N. Aqida, *IOP Conf. Ser.: Mater. Sci. Eng.*, 2019, **469**(1), 012092.
243 QED Technologies, https://qedmrf.com/en/, accessed April 2020.
244 P. Zhang, K. H. Lee and C. H. Lee, *Chin. J. Mech. Eng.*, 2016, **29**(1), 84–90.
245 P. Zhang, K. H. Lee and C. H. Lee, *J. Magn. Magn. Mater.*, 2017, **421**, 13–18.
246 K. Shahrivar, A. L. Ortiz and J. de Vicente, *Tribol. Int.*, 2014, **78**, 125–133.
247 A. J. F. Bombard, F. R. Gonçalves, K. Shahrivar, A. L. Ortiz and J. de Vicente, *Tribol. Int.*, 2015, **81**, 309–320.
248 Z. D. Hu, H. Yan, H. Z. Qiu, P. Zhang and Q. Liu, *Wear*, 2012, **278**, 48–52.
249 T. Aravind, N. Arunachalam and A. X. Kennedy, *Mater. Res. Express*, 2018, **6**(1), 016104.
250 Y. Wang, S. Yin and H. Huang, *Int. J. Adv. Des. Manuf. Technol.*, 2017, **91**(5–8), 2831–2841.
251 M. Das, V. K. Jain and P. S. Ghoshdastidar, *Int. J. Adv. Des. Manuf. Technol.*, 2012, **62**(1–4), 405–420.
252 Z. Alam and S. Jha, *Wear*, 2017, **374**, 54–62.
253 J. W. Lee, S. J. Ha, Y. K. Cho, K. B. Kim and M. W. Cho, *J. Mech. Sci. Technol.*, 2015, **29**(5), 2205–2211.
254 Z. Rigbi and L. Jilken, *J. Magn. Magn. Mater.*, 1983, **37**(3), 267–276.
255 M. R. Jolly, J. D. Carlson, B. C. Muñoz and T. A. Bullions, *J. Intell. Mater. Syst. Struct.*, 1996, **7**(6), 613–622.
256 M. Yu, B. Ju, J. Fu, X. Liu and Q. Yang, *J. Magn. Magn. Mater.*, 2012, **324**(13), 2147–2152.
257 L. C. Davis, *J. Appl. Phys.*, 1999, **85**(6), 3348–3351.
258 A. Fuchs, J. Sutrisno, F. Gordaninejad, M. B. Caglar and L. Yanming, *J. Appl. Polym. Sci.*, 2010, **117**(2), 934–942.
259 S. A. A. Aziz, S. A. Mazlan, N. I. N. Ismail, S. B. Choi, N. A. Nordin and N. Mohamad, *Smart Mater. Struct.*, 2018, **27**(11), 117002.
260 C. W. Lee, I. H. Kim and H. J. Jung, *Shock Vib.*, 2018, **2018**, 7434536.
261 C. W. Macosko, *Rheology: Principles, Measurements, and Applications*, Wiley-VCH, New York, 1994.
262 B. X. Ju, M. Yu, J. Fu, Q. Yang, X. Q. Liu and X. Zheng, *Smart Mater. Struct.*, 2012, **21**(3), 035001.
263 X. P. Do and S. B. Choi, *Shock Vib.*, 2015, 915859.
264 M. Yu, M. Zhu, J. Fu, P. A. Yang and S. Qi, *Smart Mater. Struct.*, 2015, **24**(11), 115021.
265 R. Li and L. Z. Sun, *Appl. Phys. Lett.*, 2011, **99**(13), 131912.
266 I. Agirre-Olabide, M. J. Elejabarrieta and M. M. Bou-Ali, *J. Intell. Mater. Syst. Struct.*, 2015, **26**(14), 1880–1886.
267 J. Yang, X. Gong, H. Deng, L. Qin and S. Xuan, *Smart Mater. Struct.*, 2012, **21**(12), 125015.
268 J. M. Ginder, W. F. Schlotter and M. E. Nichols, in *Proc. SPIE 4331, Smart structures and materials 2001: Damping and Isolation*, ed. D. J. Inman, International Society for Optics and Photonics, 2001, pp. 103–110.
269 M. Kallio, PhD thesis, VTT Technical Research Centre of Finland, Helsinki Univ. of Technology, 2005.
270 B. Wei, X. Gong and W. Jiang, *J. Appl. Polym. Sci.*, 2010, **116**(2), 771–778.
271 Y. Li, J. Li, T. Tian and W. Li, *Smart Mater. Struct.*, 2013, **22**(9), 095020.
272 I. Agirre-Olabide and M. J. Elejabarrieta, *J. Polym. Res.*, 2017, **24**(9), 139.
273 M. Norouzi, S. M. Sajjadi Alehashem, H. Vatandoost, Y. Q. Ni and M. M. Shahmardan, *J. Intell. Mater. Syst. Struct.*, 2016, **27**(8), 1121–1135.
274 R. Li and L. Z. Sun, *Acta Mech.*, 2014, **225**(4–5), 1347–1359.
275 I. Agirre-Olabide and M. J. Elejabarrieta, *Polym. Test.*, 2018, **66**, 114–121.
276 I. Agirre-Olabide, J. Berasategui, M. J. Elejabarrieta and M. M. Bou-Ali, *J. Intell. Mater. Syst. Struct.*, 2014, **25**(16), 2074–2081.
277 T. F. Tian, X. Z. Zhang, W. H. Li, G. Alici and J. Ding, *J. Phys.: Conf. Ser.*, 2013, **412**(1), 012038.
278 A. R. Payne, *J. Appl. Polym. Sci.*, 1962, **6**(19), 57–63.
279 C. Bellan and G. Bossis, *Int. J. Mod. Phys. B*, 2002, **16**(17–18), 2447–2453.
280 L. Bodelot, J. P. Voropaieff and T. Pössinger, *Exp. Mech.*, 2018, **58**(2), 207–221.
281 T. Pössinger, C. Bolzmacher, L. Bodelot and N. Triantafyllidis, *Microsyst. Technol.*, 2014, **20**(4–5), 803–814.
282 S. R. Khimi and K. L. Pickering, *Composites, Part B*, 2016, **90**, 115–125.
283 R. Huang, L. Wang, Y. Lin, Y. Dong and D. You, *Surf. Interface Anal.*, 2017, **49**(2), 79–84.
284 R. Damiani and L. Z. Sun, *Int. J. Damage Mech.*, 2017, **26**(1), 104–118.
285 Y. C. Fan, X. L. Gong, W. Q. Jiang, W. Zhang, B. Wei and W. H. Li, *Smart Mater. Struct.*, 2010, **19**(5), 055015.
286 L. Ge, X. Gong, Y. Fan and S. Xuan, *Smart Mater. Struct.*, 2013, **22**(11), 115029.
287 S. H. Kwon, J. H. Lee and H. J. Choi, *Materials*, 2018, **11**(6), 1040.
288 C. Wu, Q. Zhang, Y. Song and Q. Zheng, *AIP Adv.*, 2017, **7**(9), 095004.
289 G. E. Iacobescu, M. Balasoiu and I. Bica, *J. Supercond. Novel Magn.*, 2013, **26**(4), 785–792.
290 D. Günther, D. Y. Borin, S. Günther and S. Odenbach, *Smart Mater. Struct.*, 2011, **21**(1), 015005.
291 T. Borbáth, S. Günther, D. Y. Borin, T. Gundermann and S. Odenbach, *Smart Mater. Struct.*, 2012, **21**(10), 105018.
292 T. Gundermann, S. Günther, D. Borin and S. Odenbach, *J. Phys.: Conf. Ser.*, 2013, **412**(1), 012027.

Open Access Article. Published on 01 September 2020. Downloaded on 2/15/2026 12:16:02 AM.
This article is licensed under a Creative Commons Attribution 3.0 Unported Licence.

293 T. Gundermann, P. Cremer, H. Löwen, A. M. Menzel and S. Odenbach, *Smart Mater. Struct.*, 2017, **26**(4), 045012.
294 D. Borin, D. Günther, C. Hintze, G. Heinrich and S. Odenbach, *J. Magn. Magn. Mater.*, 2012, **324**(21), 3452–3454.
295 M. Schümann and S. Odenbach, *J. Magn. Magn. Mater.*, 2017, **441**, 88–92.
296 J. Yao, Y. Sun, Y. Wang, Q. Fu, Z. Xiong and Y. Liu, *Compos. Sci. Technol.*, 2018, **162**, 170–179.
297 A. Stoll, M. Mayer, G. J. Monkman and M. Shamonin, *J. Appl. Polym. Sci.*, 2014, **131**(2), 39793.
298 E. Forster, M. Mayer, R. Rabindranath, H. Böse, G. Schlunck, G. J. Monkman and M. Shamonin, *J. Appl. Polym. Sci.*, 2013, **128**(4), 2508–2515.
299 T. Hu, S. Xuan, L. Ding and X. Gong, *Mater. Des.*, 2018, **156**, 528–537.
300 N. Prem, J. C. Vega, V. Böhm, D. Sindersberger, G. J. Monkman and K. Zimmermann, *Macromol. Chem. Phys.*, 2018, **219**(18), 1800222.
301 R. A. Landa, P. Soledad Antonel, M. M. Ruiz, O. E. Pérez, A. Butera, G. Jorge, C. L. P. Oliveira and R. M. Negri, *J. Appl. Phys.*, 2013, **114**(21), 213912.
302 O. Padalka, H. J. Song, N. M. Wereley, J. A. Filer II and R. C. Bell, *IEEE Trans. Magn.*, 2010, **46**(6), 2275–2277.
303 J. L. Mietta, G. Jorge and R. M. Negri, *Smart Mater. Struct.*, 2014, **23**(8), 085026.
304 D. Y. Borin and G. V. Stepanov, *J. Intell. Mater. Syst. Struct.*, 2015, **26**(14), 1893–1898.
305 W. H. Li and X. Z. Zhang, *Smart Mater. Struct.*, 2010, **19**(3), 035002.
306 B. Nayak, S. K. Dwivedy and K. S. Murthy, *J. Intell. Mater. Syst. Struct.*, 2015, **26**(7), 830–839.
307 S. H. Kwon, C. J. Lee, H. J. Choi, K. H. Chung and J. H. Jung, *Smart Mater. Struct.*, 2019, **28**(4), 045012.
308 M. K. Shabdin, M. A. A. Rahman, S. A. Mazlan, Ubaidillah, N. M. Hapipi, D. Adiputra, S. A. A. Aziz, I. Bahiuddin and S. B. Choi, *Materials*, 2019, **12**(3), 391.
309 H. Lu, W. Wang, F. Yang, G. Wang and X. Rui, *Mater. Res. Express*, 2018, **5**(9), 095703.
310 L. Fan, G. Wang, W. Wang, H. Lu, F. Yang and X. Rui, *J. Mater. Sci.*, 2019, **54**(2), 1326–1340.
311 D. Borin, G. Stepanov and E. Dohmen, *Arch. Appl. Mech.*, 2019, **89**(1), 105–117.
312 S. A. A. Aziz, S. A. Mazlan, N. N. Ismail, M. H. A. Khairi and N. A. Yunus, *J. Phys.: Conf. Ser.*, 2017, **795**(1), 012074.
313 S. A. A. Aziz, S. A. Mazlan, N. I. N. Ismail and S. B. Choi, *J. Mater. Sci.*, 2018, **53**(14), 10122–10134.
314 U. R. Poojary, S. Hegde and K. V. Gangadharan, *J. Mater. Sci.*, 2018, **53**(6), 4229–4241.
315 V. V. Sorokin, G. V. Stepanov, M. Shamonin, G. J. Monkman and E. Y. Kramarenko, *Smart Mater. Struct.*, 2017, **26**(3), 035019.
316 S. Aloui and M. Klüppel, *Smart Mater. Struct.*, 2014, **24**(2), 025016.
317 P. R. von Lockette, S. E. Lofland, J. H. Koo, J. Kadlowec and M. Dermond, *Polym. Test.*, 2008, **27**(8), 931–935.
318 P. Siegfried, J. H. Koo and M. Pechan, *Polym. Test.*, 2014, **37**, 6–11.
319 C. J. Lee, S. H. Kwon, H. J. Choi, K. H. Chung and J. H. Jung, *Colloid Polym. Sci.*, 2018, **296**(9), 1609–1613.
320 L. A. Makarova, Y. A. Alekhina and N. S. Perov, *J. Magn. Magn. Mater.*, 2017, **440**, 30–32.
321 Q. Wen, Y. Wang and X. Gong, *Smart Mater. Struct.*, 2017, **26**(7), 075012.
322 D. Gorman, N. Murphy, R. Ekins and S. Jerrams, *Polym. Test.*, 2016, **51**, 74–81.
323 G. Liao, X. Gong and S. Xuan, *Mater. Lett.*, 2013, **106**, 270–272.
324 T. Kikuchi, Y. Kobayashi, M. Kawai and T. Mitsumata, *Int. J. Mol. Sci.*, 2018, **19**(10), 3045.
325 V. V. Sorokin, I. A. Belyaeva, M. Shamonin and E. Y. Kramarenko, *Phys. Rev. E*, 2017, **95**(6), 062501.
326 B. Sandesh, H. Sriharsha, U. R. Sathish and G. Nikhil, *MATEC Web Conf.*, 2018, **144**, 02015.
327 D. Y. Borin, G. V. Stepanov and S. Odenbach, *J. Phys.: Conf. Ser.*, 2013, **412**(1), 012040.
328 D. Borin, N. Kolsch, G. Stepanov and S. Odenbach, *Rheol. Acta*, 2018, **57**(3), 217–227.
329 N. Ghafoorianfar, X. Wang and F. Gordaninejad, *Smart Mater. Struct.*, 2014, **23**(5), 055010.
330 Y. Han, W. Hong and L. E. Faidley, *Int. J. Solids Struct.*, 2013, **50**(14–15), 2281–2288.
331 S. S. Sun, Y. Chen, J. Yang, T. F. Tian, H. X. Deng, W. H. Li, H. Du and G. Alici, *Smart Mater. Struct.*, 2014, **23**(7), 075009.
332 S. Sun, H. Deng, J. Yang, W. Li, H. Du and G. Alici, *J. Intell. Mater. Syst. Struct.*, 2015, **26**(14), 1757–1763.
333 S. Suo, Z. Xu, W. Li and Y. Gan, *J. Aerosp. Eng.*, 2018, **31**(5), 04018046.
334 J. H. Koo, F. Khan, D. D. Jang and H. J. Jung, *Smart Mater. Struct.*, 2010, **19**(11), 117002.
335 P. Małecki, M. Krolewicz, J. Krzak, J. Kaleta and J. Pigłowski, *J. Intell. Mater. Syst. Struct.*, 2015, **26**(14), 1899–1905.
336 M. Norouzi, M. Gilani, S. S. Alehashem and H. Vatandoost, *IEEE Trans. Magn.*, 2017, **53**(9), 1–12.
337 F. Guo, C. B. Du and R. P. Li, *Adv. Mech. Eng.*, 2014, **6**, 629386.
338 S. Qi, M. Yu, J. Fu, P. D. Li and M. Zhu, *Smart Mater. Struct.*, 2015, **25**(1), 015020.
339 S. Qi, M. Yu, J. Fu and M. Zhu, *J. Intell. Mater. Syst. Struct.*, 2018, **29**(2), 205–213.
340 K. Danas, S. V. Kankanala and N. Triantafyllidis, *J. Mech. Phys. Solids*, 2012, **60**(1), 120–138.
341 J. Feng, S. Xuan, T. Liu, L. Ge, L. Yan, H. Zhou and X. Gong, *Smart Mater. Struct.*, 2015, **24**(8), 085032.
342 Y. Wan, Y. Xiong and S. Zhang, *Compos. Struct.*, 2018, **202**, 768–773.
343 Y. Tao, X. Rui, F. Yang, G. Chen, L. Bian, W. Zhu and M. Wei, *J. Intell. Mater. Syst. Struct.*, 2018, **29**(7), 1418–1429.
344 D. Leng, T. Wu, G. Liu, X. Wang and L. Sun, *J. Intell. Mater. Syst. Struct.*, 2018, **29**(10), 2236–2248.
345 H. Vatandoost, M. Norouzi, S. M. S. Alehashem and S. K. Smoukov, *Smart Mater. Struct.*, 2017, **26**(6), 065011.

This journal is © The Royal Society of Chemistry 2020

Open Access Article. Published on 01 September 2020. Downloaded on 2/15/2026 12:16:02 AM. This article is licensed under a Creative Commons Attribution 3.0 Unported Licence.

346 G. Schubert and P. Harrison, *Smart Mater. Struct.*, 2016, **25**(1), 015015.
347 G. Schubert and P. Harrison, *J. Magn. Magn. Mater.*, 2016, **404**, 205–214.
348 D. Leng, L. Sun, J. Sun, W. Chen, F. Ma, W. Li and Y. Lin, *J. Phys.: Conf. Ser.*, 2013, **412**(1), 012029.
349 L. Chen and S. Jerrams, *J. Appl. Phys.*, 2011, **110**(1), 013513.
350 A. M. Biller, O. V. Stolbov and Y. L. Raikher, *J. Appl. Phys.*, 2014, **116**(11), 114904.
351 A. M. Biller, O. V. Stolbov and Y. L. Raikher, *Phys. Rev. E: Stat., Nonlinear, Soft Matter Phys.*, 2015, **92**(2), 023202.
352 M. V. Vaganov, D. Y. Borin, S. Odenbach and Y. L. Raikher, *J. Magn. Magn. Mater.*, 2018, **459**, 92–97.
353 A. M. Menzel, *Arch. Appl. Mech.*, 2019, **89**(1), 17–45.
354 G. Pessot, H. Löwen and A. M. Menzel, *J. Chem. Phys.*, 2016, **145**(10), 104904.
355 G. Pessot, M. Schümann, T. Gundermann, S. Odenbach, H. Löwen and A. M. Menzel, *J. Phys.: Condens. Matter*, 2018, **30**(12), 125101.
356 W. Li, X. Zhang, T. Tian and W. Wen, *AIP Conf. Proc.*, 2013, **1542**(1), 129–132.
357 S. H. Kim, Y. J. Park, A. R. Cha, G. W. Kim, J. H. Bang, C. S. Lim and S. B. Choi, *IOP Conf. Ser.: Mater. Sci. Eng.*, 2018, **333**(1), 012013.
358 S. Lee, C. Yim, W. Kim and S. Jeon, *ACS Appl. Mater. Interfaces*, 2015, **7**(35), 19853–19856.
359 V. V. Sorokin, B. O. Sokolov, G. V. Stepanov and E. Y. Kramarenko, *J. Magn. Magn. Mater.*, 2018, **459**, 268–271.
360 S. Chen, S. Dong, X. Wang and W. Li, *Smart Mater. Struct.*, 2019, **28**, 045016.
361 J. P. Déry, D. Brousseau, M. Rochette, E. F. Borra and A. M. Ritcey, *J. Appl. Polym. Sci.*, 2017, **134**(9), 44542.
362 D. Chen, A. Song, X. Hu, L. Fu and Q. Ouyang, *IEEE Access*, 2019, **7**, 15125–15139.
363 M. Sedlačík, M. Mrlík, V. Babayan and V. Pavlínek, *Compos. Struct.*, 2016, **135**, 199–204.
364 M. Cvek, R. Moucka, M. Sedlačík, V. Babayan and V. Pavlínek, *Smart Mater. Struct.*, 2017, **26**(9), 095005.
365 L. R. Wang, M. Yu, P. A. Yang, S. Qi and J. Fu, *Smart Mater. Struct.*, 2019, **28**(4), 044001.
366 R. Moucka, M. Sedlačík and M. Cvek, *Appl. Phys. Lett.*, 2018, **112**(12), 122901.
367 H. Zhong, Y. Pei, Z. Hu, P. Zhang, J. Guo, X. Gong and Y. Zhao, *Smart Mater. Struct.*, 2019, **28**(2), 025027.
368 X. Zhu, Y. Meng and Y. Tian, *Smart Mater. Struct.*, 2010, **19**(11), 117001.
369 S. M. Hasheminejad and M. Shabanimotlagh, *Smart Mater. Struct.*, 2010, **19**(3), 035006.
370 A. R. Baev, E. V. Korobko and Z. A. Novikova, *J. Intell. Mater. Syst. Struct.*, 2015, **26**(14), 1913–1919.
371 R. Elhajjar, C. T. Law and A. Pegoretti, *Prog. Mater. Sci.*, 2018, **97**, 204–229.
372 S. Qi, H. Guo, J. Chen, J. Fu, C. Hu, M. Yu and Z. L. Wang, *Nanoscale*, 2018, **10**(10), 4745–4752.
373 M. Behrooz and F. Gordaninejad, *Smart Mater. Struct.*, 2016, **25**(2), 025011.
374 S. Y. Tang, X. Zhang, S. Sun, D. Yuan, Q. Zhao, S. Yan, L. Deng, G. Yun, J. Zhang, S. Zhang and W. Li, *Adv. Funct. Mater.*, 2018, **28**(8), 1705484.
375 A. Ehsani and A. Nejat, *Smart Mater. Struct.*, 2017, **26**(5), 055036.
376 G. Diguet, E. Beaugnon and J. Y. Cavaillé, *Smart Mater. Struct.*, 2012, **21**(2), 025016.
377 X. Gong, G. Liao and S. Xuan, *Appl. Phys. Lett.*, 2012, **100**(21), 211909.
378 O. V. Stolbov, Y. L. Raikher and M. Balasoiu, *Soft Matter*, 2011, **7**(18), 8484–8487.
379 R. Li, D. Ren, X. Wang, X. Chen, S. Chen and X. Wu, *J. Intell. Mater. Syst. Struct.*, 2018, **29**(2), 160–170.
380 C. Lian, K. H. Lee and C. H. Lee, *Tribol. Int.*, 2016, **98**, 292–298.
381 C. Lian, K. H. Lee, J. W. An and C. H. Lee, *Friction*, 2017, **5**(4), 383–391.
382 E. Psarra, L. Bodelot and K. Danas, *Soft Matter*, 2017, **13**(37), 6576–6584.
383 S. Wang, W. Jiang, W. Jiang, F. Ye, Y. Mao, S. Xuan and X. Gong, *J. Mater. Chem. C*, 2014, **2**(34), 7133–7140.
384 H. An, S. J. Picken and E. Mendes, *Polymer*, 2012, **53**(19), 4164–4170.
385 H. Pang, L. Pei, C. Sun and X. Gong, *J. Rheol.*, 2018, **62**(6), 1409–1418.
386 P. J. Rankin, A. T. Horvath and D. J. Klingenberg, *Rheol. Acta*, 1999, **38**(5), 471–477.
387 B. O. Park, B. J. Park, M. J. Hato and H. J. Choi, *Colloid Polym. Sci.*, 2011, **289**(4), 381–386.
388 J. P. Rich, G. H. McKinley and P. S. Doyle, *Langmuir*, 2012, **28**(8), 3683–3689.
389 H. Wang, Y. Li, G. Zhang and J. Wang, *Smart Mater. Struct.*, 2019, **28**(3), 035002.
390 J. Yang, H. Yan, J. Dai, Z. Hu and H. Zhang, *J. Rheol.*, 2017, **61**(3), 515–524.
391 J. Whiteley, F. Gordaninejad and X. Wang, *J. Appl. Mech.*, 2010, **77**(4), 041011.
392 P. Yang, M. Yu and J. Fu, *J. Nanopart. Res.*, 2016, **18**(3), 61.
393 M. Yu, H. Luo, J. Fu and P. Yang, *J. Intell. Mater. Syst. Struct.*, 2018, **29**(1), 24–31.
394 P. Yang, M. Yu, H. Luo, J. Fu, H. Qu and Y. Xie, *Appl. Surf. Sci.*, 2017, **416**, 772–780.
395 H. Zhang, H. Yan, Z. Hu, J. Yang and F. Niu, *J. Magn. Magn. Mater.*, 2018, **451**, 102–109.
396 S. Xuan, Y. Xu, T. Liu and X. Gong, *Int. J. Smart Nano Mater.*, 2015, **6**(2), 135–148.
397 T. Liu, X. Gong, Y. Xu, H. Pang and S. Xuan, *Smart Mater. Struct.*, 2014, **23**(10), 105028.
398 X. Gong, Y. Xu, S. Xuan, C. Guo, L. Zong and W. Jiang, *J. Rheol.*, 2012, **56**(6), 1375–1391.
399 T. Liu, Y. Xu, X. Gong, H. Pang and S. Xuan, *AIP Adv.*, 2013, **3**(8), 082122.
400 Y. Xu, X. Gong, T. Liu and S. Xuan, *J. Rheol.*, 2014, **58**(3), 659–679.
401 J. Xu, S. Xuan, H. Pang and X. Gong, *Smart Mater. Struct.*, 2017, **26**(3), 035044.

Open Access Article. Published on 01 September 2020. Downloaded on 2/15/2026 12:16:02 AM.
This article is licensed under a Creative Commons Attribution 3.0 Unported Licence.

402 J. Xu, P. Wang, H. Pang, Y. Wang, J. Wu, S. Xuan and X. Gong, *Compos. Sci. Technol.*, 2018, **159**, 50–58.
403 B. X. Ju, M. Yu, J. Fu, Q. Yang, X. Q. Liu and X. Zheng, *Smart Mater. Struct.*, 2012, **21**(3), 035001.
404 T. Plachý, O. Kratina and M. Sedlačík, *Compos. Struct.*, 2018, **192**, 126–130.
405 J. D. Carlson and M. R. Jolly, *Mechatronics*, 2000, **10**(4-5), 555–569.
406 S. S. Deshmukh and G. H. McKinley, *Smart Mater. Struct.*, 2006, **16**(1), 106.
407 T. G. Zielinski and M. Rak, *J. Intell. Mater. Syst. Struct.*, 2010, **21**(2), 125–131.
408 E. Dohmen, M. Boisly, D. Borin, M. Kästner, V. Ulbricht, M. Gude, W. Hufenbach, G. Heinrich and S. Odenbach, *Adv. Eng. Mater.*, 2014, **16**(10), 1270–1275.
409 L. Ge, S. Xuan, G. Liao, T. Yin and X. Gong, *Smart Mater. Struct.*, 2015, **24**(3), 037001.
410 J. Gan, X. He, G. Zhang, C. Zhou, Q. Zheng, C. Gao and H. Wang, *IOP Conf. Ser.: Mater. Sci. Eng.*, 2017, **231**(1), 012168.
411 D. Bodniewicz, J. Kaleta and D. Lewandowski, *Compos. Struct.*, 2018, **189**, 177–183.
412 S. K. Reddy, A. Mukherjee and A. Misra, *Appl. Phys. Lett.*, 2014, **104**(26), 261906.
413 X. Liu, X. Gao, H. Yu and D. Ye, *IEEE Trans. Magn.*, 2015, **51**(10), 1–5.
414 X. Yao, C. Liu, H. Liang, H. Qin, Q. Yu and C. Li, *J. Magn. Magn. Mater.*, 2016, **403**, 161–166.
415 D. York, X. Wang and F. Gordaninejad, *J. Intell. Mater. Syst. Struct.*, 2007, **18**, 1221–1225.
416 X. Wang and F. Gordaninejad, *Smart Mater. Struct.*, 2009, **18**, 095045.
417 A. K. Bastola, L. Li and M. Paudel, *J. Mater. Sci.*, 2018, **53**(9), 7004–7016.
418 A. K. Bastola, M. Paudel and L. Li, *Polymer*, 2018, **149**, 213–228.
419 J. de Vicente and C. L. Berli, *Rheol. Acta*, 2013, **52**(5), 467–483.
420 L. Shan, K. Chen, M. Zhou, X. Zhang, Y. Meng and Y. Tian, *Smart Mater. Struct.*, 2015, **24**(10), 105030.
421 N. Caterino, M. Spizzuoco and A. Occhiuzzi, *Smart Mater. Struct.*, 2018, **27**(6), 067001.
422 A. Fuchs, A. Rashid, Y. Liu, B. Kavlicoglu, H. Sahin and F. Gordaninejad, *J. Appl. Polym. Sci.*, 2010, **115**(6), 3348–3356.
423 M. McKee, F. Gordaninejad and X. Wang, *J. Intell. Mater. Syst. Struct.*, 2018, **29**(1), 41–51.
424 M. C. Heine, J. de Vicente and D. J. Klingenberg, *Phys. Fluids*, 2006, **18**(2), 023301.
425 G. Cha, Y. S. Ju, L. A. Ahuré and N. M. Wereley, *J. Appl. Phys.*, 2010, **107**(9), 09B505.
426 I. de Vicente, A. Merino-Martos, L. Cruz-Pizarro and J. de Vicente, *J. Hazard. Mater.*, 2010, **181**, 375–381.
427 I. Singh, C. S. Lacko, Z. Zhao, C. E. Schmidt and C. Rinaldi, *J. Colloid Interface Sci.*, 2020, **561**, 647–658.
428 G. Peng, Y. Ge, J. Ding, C. Wang, G. G. Wallace and W. Li, *Smart Mater. Struct.*, 2018, **27**(3), 035022.

 This journal is © The Royal Society of Chemistry 2020